DNA Tension Probes Show that Cardiomyocyte Maturation Is Sensitive to the pN Traction Forces Transmitted by Integrins

Sk Aysha Rashid[1]; Aaron T Blanchard[3]; J Dale Combs[1]; Natasha Fernandez[2]; Yixiao Dong[1]; Hee Cheol Cho[2,3]; and Khalid Salaita[1,3]*.

[1]Department of Chemistry, Emory University, 1515 Dickey drive, Atlanta GA 30322,USA
[2]Division of Pediatric Cardiology, Department of Pediatrics, Emory University School of Medicine and Children's Healthcare of Atlanta, 1405 Clifton Rd NE, Atlanta GA 30322,USA
[3]Wallace H. Coulter Department of Biomedical Engineering, Georgia Institute of Technology and Emory University, 313 Ferst Drive, Atlanta GA 30332, USA

*Corresponding author. Khalid Salaita

Email: k.salaita@emory.edu

Table of Contents

1) Determination of rupture probability

Rupture probability (p_{rup}) vs. force plots shown in Fig. 1c were calculated from the force-induced rupture rate, k_{rup}:

$$p_{rup} = 1 - \exp(-k_{rup}\Delta t)$$

where Δt is the duration of constantly applied force. The parameter k_{rup} was approximated using Bell's model[1]:

$$k_{rup} = k_0 \exp\left(\frac{F\, x_{tst}}{k_B T}\right)$$

where F is the applied force, $k_B T = 4.114\, pN\, nm$ is the thermal energy at room temperature, k_0 is the zero-force off rate, and x_{tst} is the distance to transition state parameter. T_{tol} is generally defined as the constantly applied force that results in $p_{rup} = 0.5$ when $\Delta t = 2\, s$, which can be solved for by re-arranging the previous two equations and substituting T_{tol} for F:

$$T_{tol} = \frac{k_B T}{x_{tst}} \ln\left(\frac{ln(2)}{k_0(2\, s)}\right)$$

For all three tension sensors, we used $k_0 = 10^{-6}$ to reflect a very low rate of dissociation at zero force[2, 3] and calculated x_{tst} as the value that produced the previously calibrated T_{tol} when $\Delta t = 2\, s$.

2) Determination of DNA surface density

To measure the DNA density on the surface we followed a previously reported surface density measurement assay.[4]The protocol allows one to convert the raw fluorescence intensity of the surface to the molecular density of fluorescent molecules. In this assay, lipid membranes were used as calibrated fluorescence standards, based on the known documented molecular density of phospholipids within membranes. In this calibration, the intensity of labeled oligonucleotides and small unilamellar vesicles (SUVs) in solution are compared to determine the F factor, which relates molecular brightness of the two fluorophores. The concentration of rupture probes on surface was calculated using F factor. It was done by calibration curve generated by imaging known concentrations of supported lipid bilayers (SLBs). To prepare SLBs, SUVs were prepared by mixing 99.9 mol% 1,2-dioleoyl-sn-glycero-3-phosphocholine (DOPC) and 0.1 mol% Texas Red 1,2 dihexadecanoyl-sn-glycero-3-phosphoethanolamine, triethylammonium salt (TR-DHPE, T1395MP, Thermofisher Scientific) in a round bottom flask with chloroform. Lipids were dried for 30 min under rotary evaporation followed by an ultra-high-purity nitrogen stream to remove residual chloroform. The dried lipid film was hydrated with nanopure water (2 mg/mL) before conducting three freeze-thaw cycles. The mixture was then passed through 10mL LIPEX® thermobarrel extruder 10 times (Evonik Industries, Essen, Germany) using a 80 nm polycarbonate filter. We then prepared known concentrations of labeled oligonucleotides and SUVs in solution to compare the fluorescence intensity with density. Glass was passivated with 0.1% BSA in PBS for 20-30 min. The quality of the calibration curve for DNA and SUVs was assessed by measuring the linear regression between the concentration of the known oligonucleotide (or the SUV sample) and its fluorescence intensity, as deviations can indicate nonspecific adsorption. The ratio of the calibration curve slopes was used to determine the "F factor" for the labeled oligonucleotide and the SUV samples. The F-factor was calculated as follows: $F = I_{Cy3B-DNA}/I_{TR-DHPE}$, where $I_{Cy3B-DNA}$ and $I_{TR-DHPE}$ represent the fluorescence intensities of the DNA and SUV samples, respectively. To prepare SUVs in glass bottom plates, the glass was treated with a 2 M NaOH etching solution. It was then thoroughly washed with water and 1x PBS. To create a fluorescence calibration curve,

SLBs with varying fluorophore concentration were prepared by adding mixtures of labeled and unlabeled SUVs in known stoichiometries. Excess SUVs were rinsed using 1XPBS. The intensity of the SLBs was measured using epifluorescence microscopy. Using the known lipid footprint[4] (0.72 nm^2), the generated graph was used to relate the density of fluorophores to arbitrary fluorescence units. The equation of the calculation generated for **Figure S4**, is $DNA\ density = 2 \times intensity \div (F \times slope)$. This equation was then used to convert the fluorescence intensity of DNA to probes density per μm^2.

3) α-actinin puncta analysis

Fluorescent α-actinin micrographs where subjected to image analysis using the Fiji ImageJ distribution (NIH). α-actinin micrographs were first subjected to a rolling ball background subtraction using a 15-pixel radius. Images were then converted to 8-bit greyscale images. The setAutoTHreshold ("Default dark") function was executed to enhance the contrast of the fluorescent micrograph. Next, the cell RICM ROI was selected, and the run ("Clear Outside") function was carried out to remove fluorescent signal outside of the cell area. Images were then set between 35 and 255 greyscale units. Then the run ("Convert to Mask") function was carried out, followed by the run("Watershed") function. Actinin puncta were then identified by using the "Analyze Particles" function, selecting particles between 8- and 350-pixel units. The list of actinin puncta ROIs within the cell were then saved. Finally, the number of identified puncta per cell were counted. Additionally, we used SarcOptim plugin in ImageJ to analyze the sarcomere length.[5]

4) PEG-DNA probe gel preparation

The PEG gel surface was made by mixing two precursor solutions. The first solution was made by dissolving 55 mg of 4-arm-PEG-NH$_2$ (Mw ~5k; Biopharma PEG, 10225) into 500 µL potassium phosphate buffer (pH~6.4). The second solution was made by dissolving 50 mg 4-arm-PEG-NHS molecule (Mw~5k; NOF America Corp. PTE05GS) into 500 µL potassium phosphate buffer (pH~6.4). Both the solutions were then cooled in an ice bath for 15 min before vigorous mixing using a stir bar (~400 rpm for 5s). Then 20 µL of the mixture was filled in the gap between a parafilm strip and an APTES treated glass surface to form a thin (~80 μm) hydrogel layer and incubated for 1hr at RT. After the gelation, the parafilm strip was peeled off from the PEG gel using tweezers. The gel was then vigorously washed with DMSO for 5 min and incubated with 200 µL of 3mg/mL NHS-biotin in DMSO overnight. The biotin coated peg surface was thoroughly washed with DMSO(3X), EtOH (3X), Nano-pure water(3X) and 1XPBS (3X) before incubating with 0.1mg/mL of streptavidin for 2 hr. The surface was then washed three times with 1XPBS, and 300 nM DNA was incubated for 2hr. The gel was thoroughly washed with PBS (3X) and cell culture media (3X) before seeding the NRVMs. The elastic modulus of the gel was measured using rheology and was shown to be 10-13 kPa (Figure S27b) To ensure comparable DNA densities on the PEG gel as that of the glass substrates, we collected fluorescence images of the surface at $t =$ 0 hrs (before cell seeding) (Figure S27d). CMCs were incubated for 48 hrs, and images were taken every 12 hrs to assess the attachment and morphology of the CMCs. We noted the loss of DNA as to nuclease/protease activity and biotin-SA dissociation over 48hrs of incubation with CMCs (Figure S27g).

Table 1: Identification and sequence of oligonucleotides used in this work

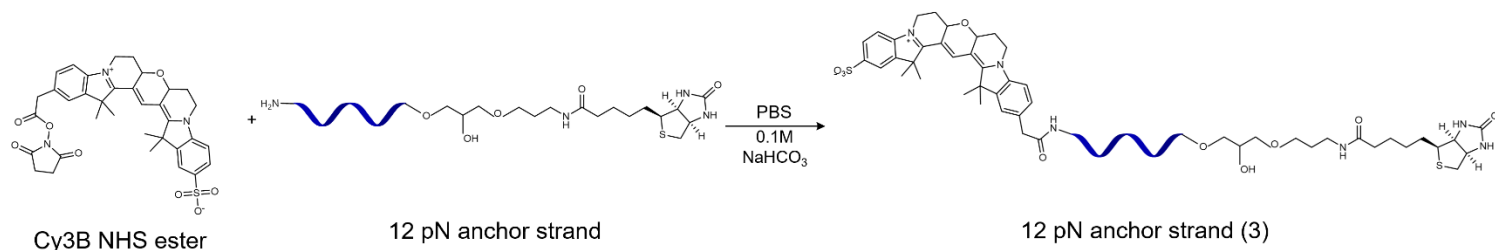| ID	DNA Sequence (5'-3')
12/56 pN ligand strand	/5Hexynyl/GTG AAA TAG CGC ACA GAT GCG /3AmMO/
56 pN anchor strand	/5Biosg/TTT/iAmMC6T/C GCA TCT GTG CGG TAT TTC AC/3/
12 pN anchor strand	/5AmMC6/CGC ATC TGT GCG GTA TTT CAC TTT/3Bio/
Biotin rupture strand	/5Hexynyl/CGC ATC TGT GCG GTA TTT CAC /iAmMC6T/TT T/3Bio/
Biotin rupture strand complement	/5/GTG AAA TAG CGC ACA GAT GCG /3/
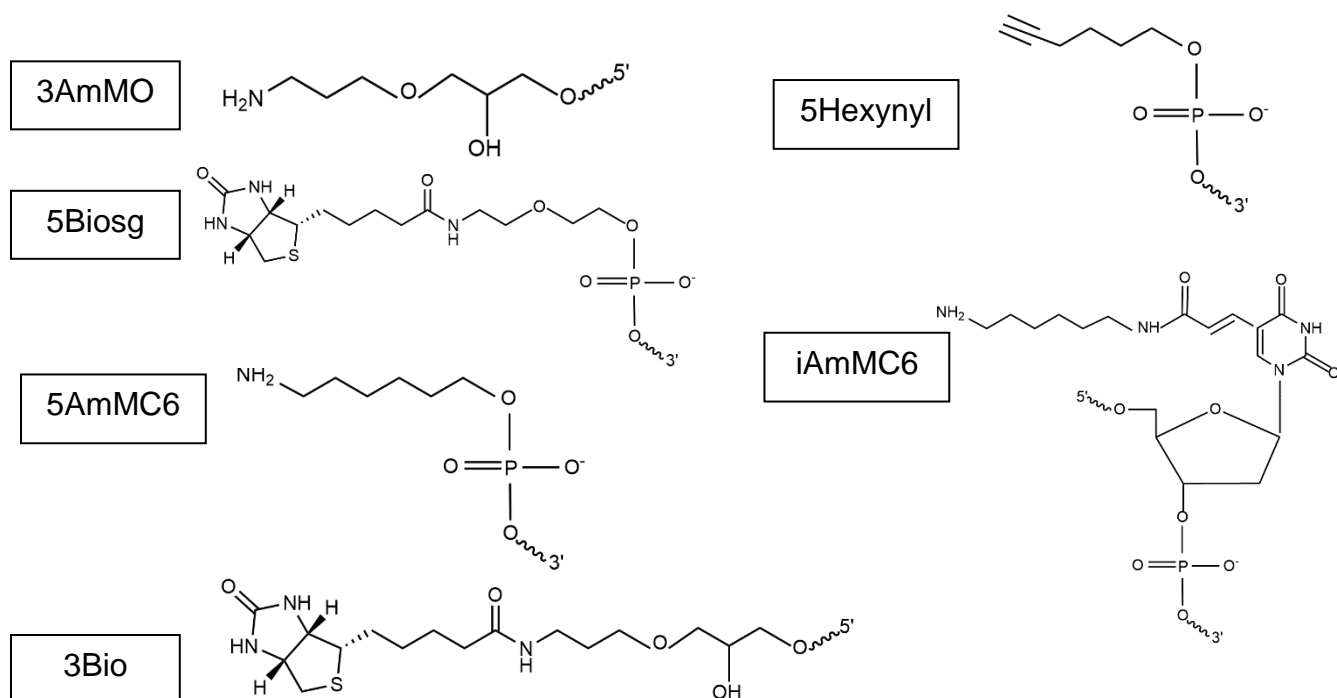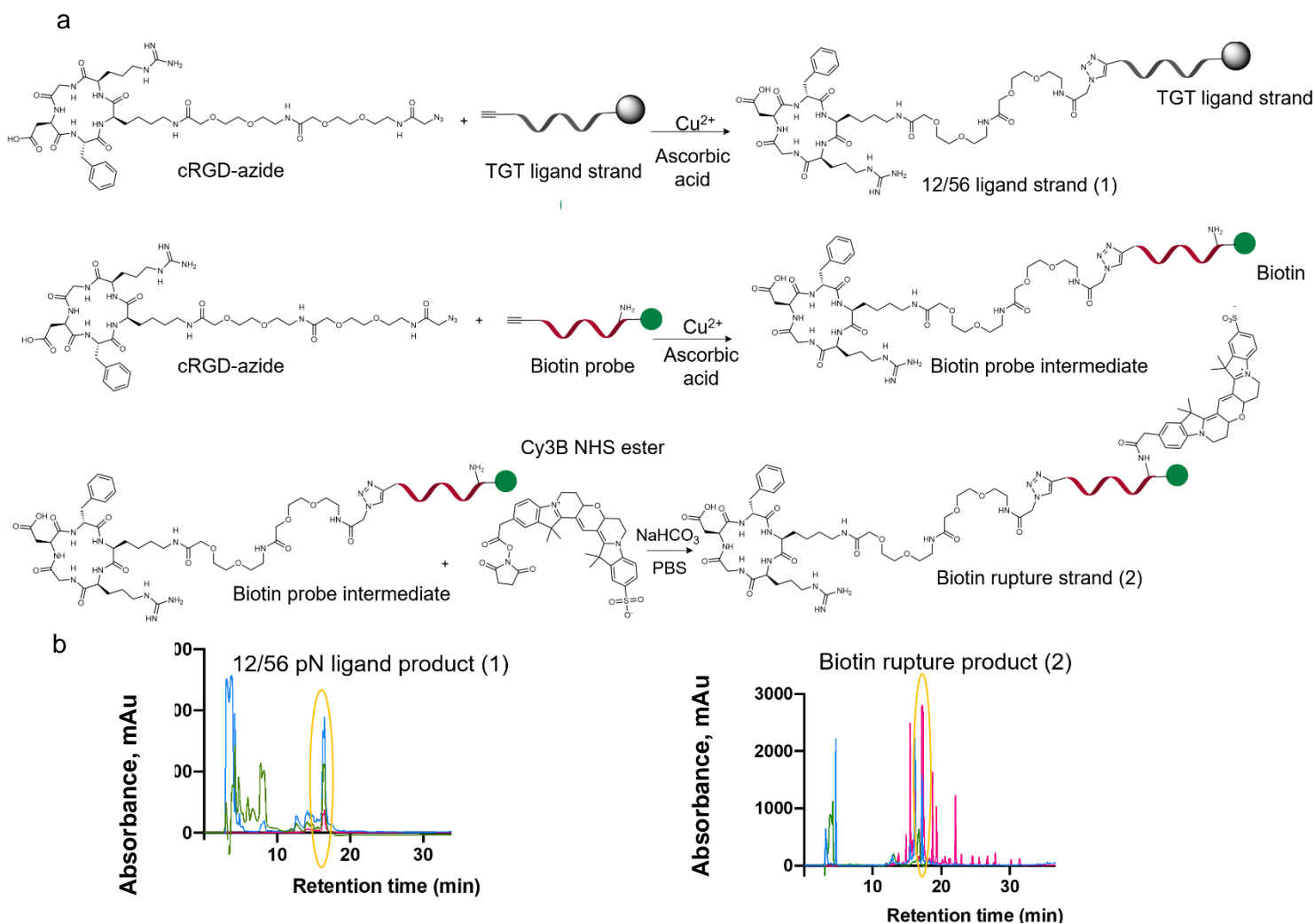
Supplementary Figure 1. Synthesis of ligand strands. a. Synthesis of 12/56 pN ligand strands. Schematic illustration of the Cu^{2+} catalyzed click reaction between the cRGD-azide and alkyne modified DNA. To prepare the biotin 12/56 pN ligand strand, the RGD peptide was first coupled to the nucleic acid followed by HPLC purification and then coupling of the peptide-nucleotide product to Cy3B dye. b. and c. Representative chromatograms of products **1** and **2.** HPLC was used to isolate and purify the products which were confirmed by mass spectrometry.

a

Cy3B NHS ester　　　　12 pN anchor strand　　　　　　　　　　12 pN anchor strand (3)

PBS
0.1M
NaHCO₃

b

Cy3B NHS ester　　　　56 pN anchor strand

PBS
0.1M
NaHCO₃

c

56 pN anchor strand (4)

12 pN anchor strand (3)

— 260(DNA)
— 575(Cy3B)
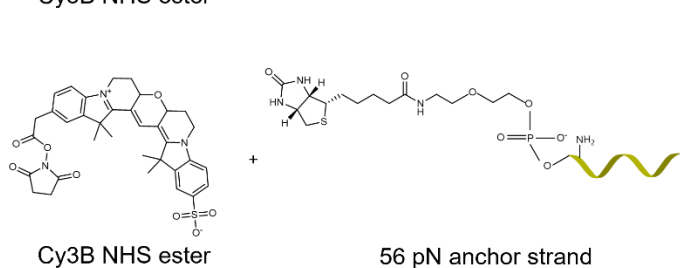
56 pN anchor strand (4)

Supplementary Figure 2: Synthesis of anchor strands. a. Schematic illustration of the NHS-NH$_2$ coupling reaction between 12 and 56 pN anchor strands and Cy3B-NHS ester. b. and c. Representative chromatograms of products **3** and **4.** HPLC was used to isolate and purify the products which were confirmed by mass spectrometry.
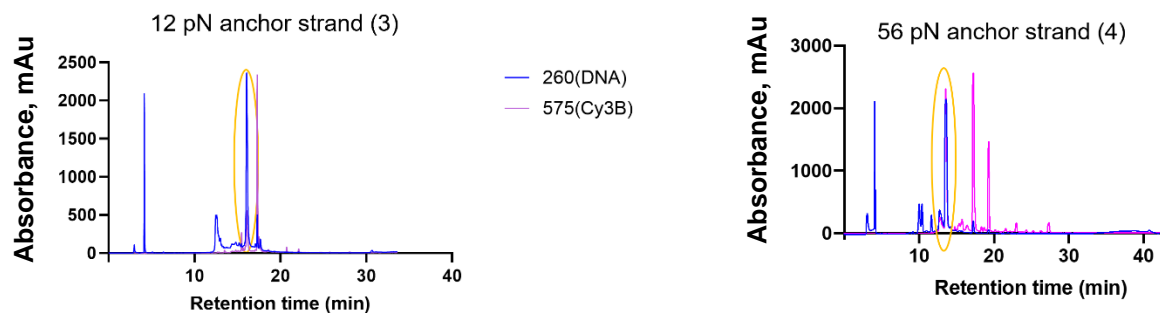
Supplementary Table 2: Expected and calculated mass of oligonucleotides

Oligo ID	Theoretical Mass	Calculated Mass (From Mass Spec)	Percent Error (%)
12 pN anchor strand	8460.6	8456.608	0.00047
56 pN anchor strand	10271.9	10266.872	0.00048
12/56 pN ligand strand	9880.9	9871.87	0.00091
Biotin rupture strand	8195.7	8190.788	0.00060

$$Quenching\ Efficiency = \left(1 - \frac{Quenched\ intensity - Background\ CCD}{Un-quenched\ intensity - Background\ CCD}\right) \times 100$$

Probes	QE
12 pN	90.2±1.2
56 pN	91.1±1.3
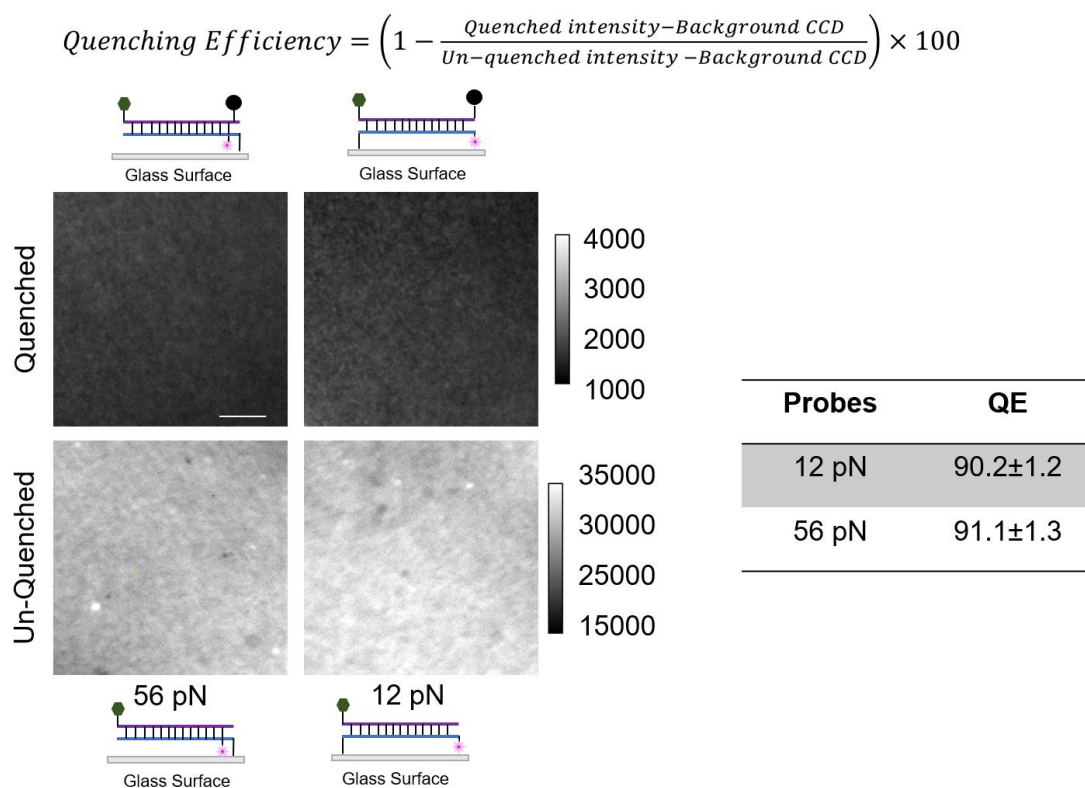
Supplementary Figure 3. Quenching efficiency measurement. Equation used to determine the quenching efficiency of 12 and 56 pN DNA probes. The quenched intensity was measured from the intensity of a uniform monolayer of probe with the Cy3B-BHQ-2 pair. The un-quenched intensity was determined from an identical monolayer of DNA probes lacking the BHQ-2 quencher. Intensities were background corrected. Scale bar = 10 μm. The error represents the standard deviation and was measured from 9 different substrates that were generated from three separate preparations

Density calibration curve
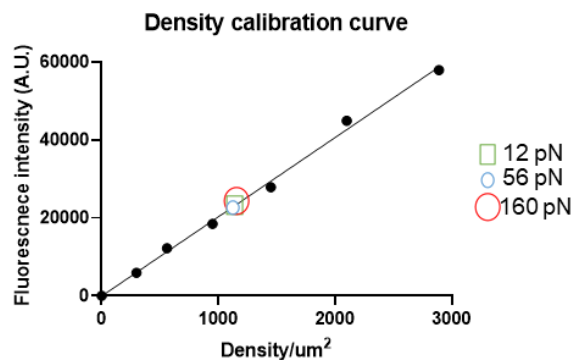
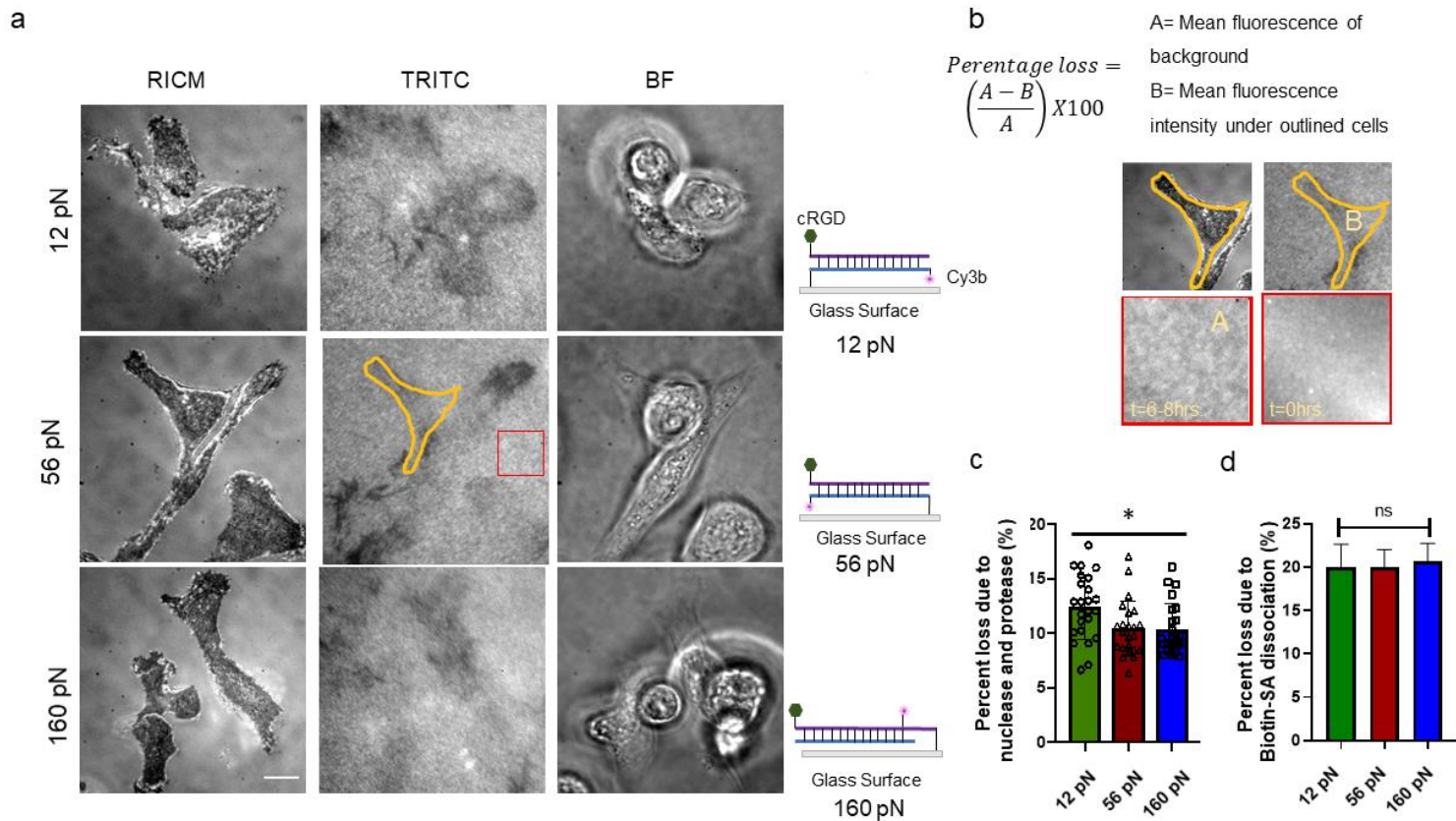| Type of TGT	Density
12 pN	1289.5 ± 55
56 pN	1238.3 ± 63
160 pN	1395.8 ± 75
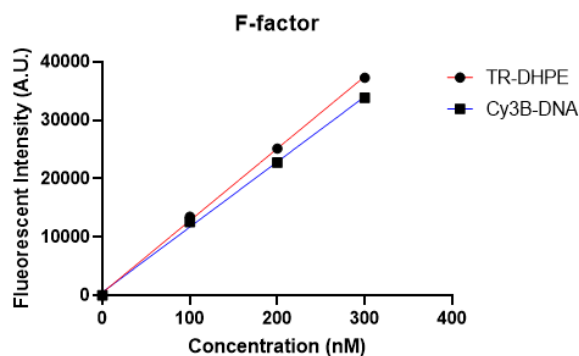
$$F = \frac{I_{Cy3B\ DNA}}{I_{TR\ DHPE}}$$

Supplementary Figure 4. Calibration curve used for determining molecular density of probes. Plot shows a calibration curve relating the fluorescence intensity of TR-DHPE – doped supported lipid membranes as a function of dye density. The density was calculated based on the mol %of the dye and by using the published density of DOPC reported using neutron scattering experiments. An F factor was also measured by comparing the calibration curve for TR-DHPE against a calibration curve for the Cy3B DNA probe. Finally, by using the TR-DHPE calibration curve along with the F factor, we were able to infer the molecular density of the 12 pN, 56 pN and 160 pN DNA probes (shown in the table). The errors signify the SD (standard deviation) from three individual replicates.
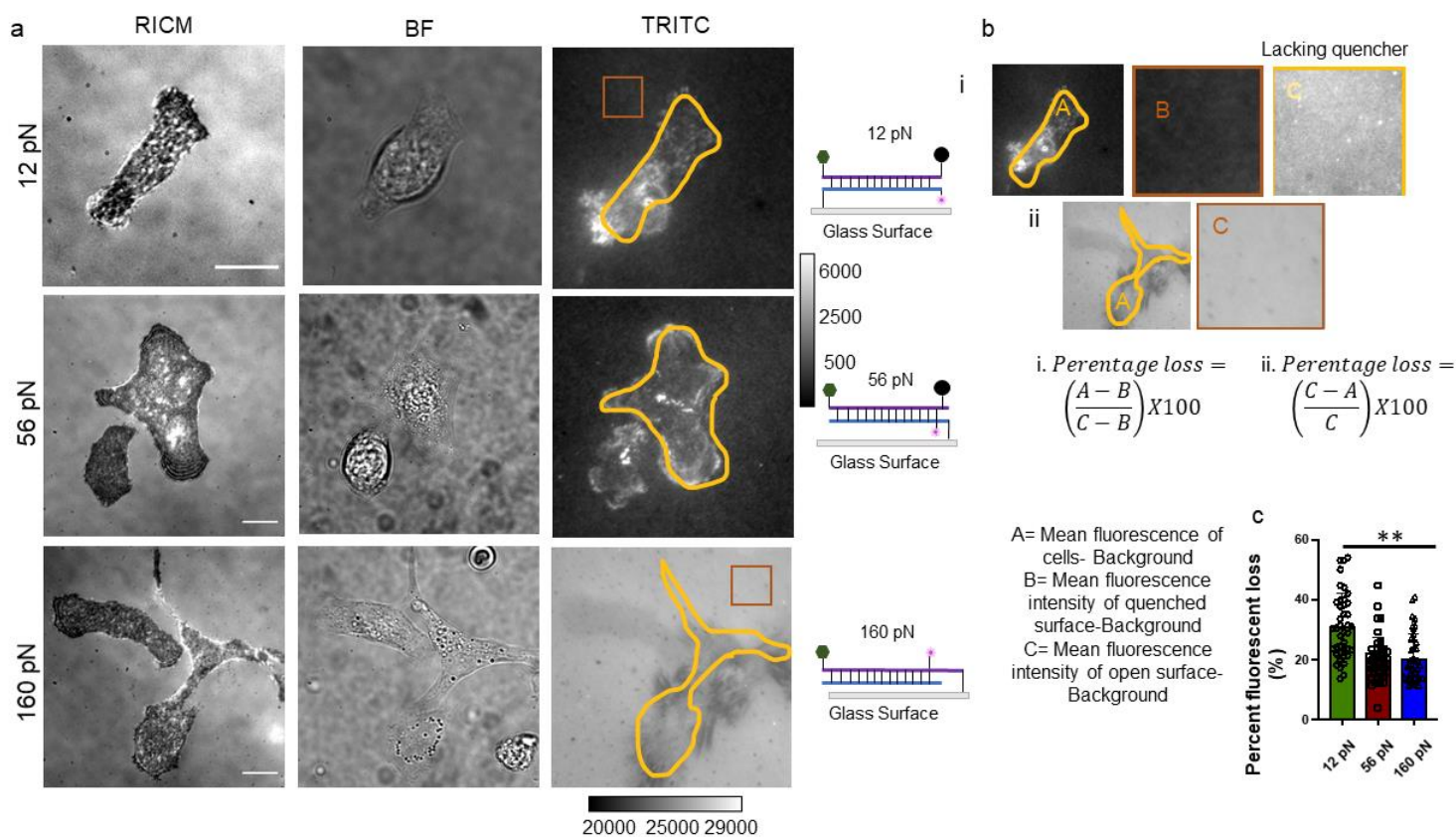
Supplementary Figure 5. Determination of fraction of DNA denatured under cells. a. representative RICM, brightfield and tension (TRITC) images of CMCs on 12, 56 and 160 pN surfaces. b. i. Representative images showing the workflow used to determine the fraction of DNA ruptured under cells on 12 and 56 pN probes. We created an ROI manually based on the RICM image (A) and also a second ROI corresponding to the signal intensity of a surface lacking quencher(C). The background regions surrounding the cell correspond to 0% ruptured probe(B), while (C) provides the mean intensity corresponding to 100% ruptured probe. Using the equation (i) we measured the loss of ligand. ii. For 160 pN probe we measured the loss of ligand by using (ii). c. Bar graph plotting the percentage of DNA probes ruptured on 12, 56 and 160 pN surfaces. Error bars represent the standard deviation from n = 3 independent surfaces for each group. Scale bar = 12 μm.

The equation shown in panel b:

$$Percentage\ loss = \left(\frac{A - B}{A}\right) X100$$

A = Mean fluorescence of background

B = Mean fluorescence intensity under outlined cells

Supplementary Figure 6. **Non-force-induced loss of DNA probes**. a. Representative RICM, Cy3B and brightfield images of CMCs cultured on 12, 56 and 160 pN surfaces for 6-8 hrs on probes lacking quencher (100% Cy3B). b. Representative images showing the workflow and the equation used to determine the probe loss due to non-mechanical events. c. Bar graph plotting DNA loss on 12, 56 and 160 pN surfaces after 6-8 hrs of incubation. This value was determined by drawing an ROI of the cell based on the RICM channel and then averaging the signal under the cell compared to the signal outside of the cell. Because DNA rupture does not lead to loss of Cy3B signal, we ascribe this loss of signal to nuclease or protease activity as well as the spontaneous dissociation of biotin-streptavidin. d. Bar graph plotting loss of signal due to biotin-streptavidin dissociation over t= 6-8hrs. (**** indicates p<0.0001 respectively from one way ANOVA.) Error bars show standard deviation for n=3 where the experiments were conducted from three different cell isolation with three different sets of surface preparation. Scale bar = 12 μm.
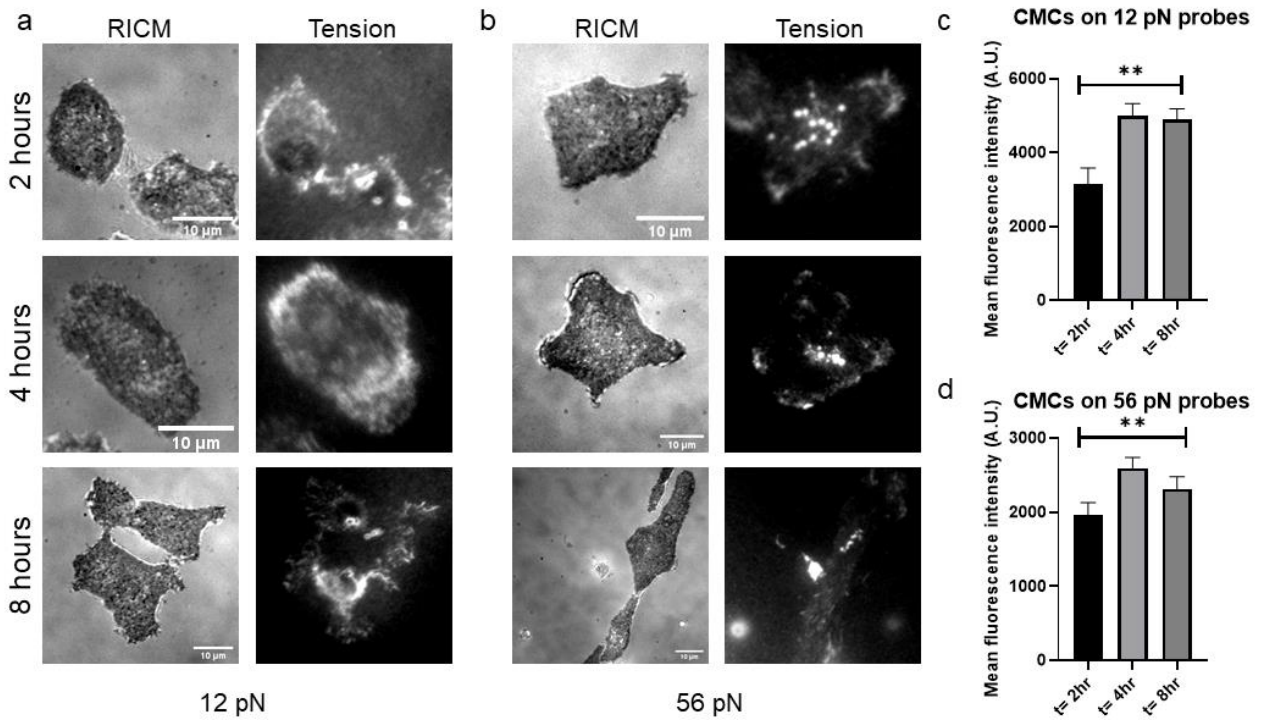
Supplementary Figure 7. Tension signal is observed prior to initiation of twitching for CMCs. a-b. Representative RICM and tension images of CMCs on 12 and 56 pN rupture probes. (c-d) Bar graph showing mean tension signal per cell as a function of seeding time for the 12 and 56 pN probes. **represents p<0.01, *n* = 3 independent experiments. Scale bar= 10 *μ*m.
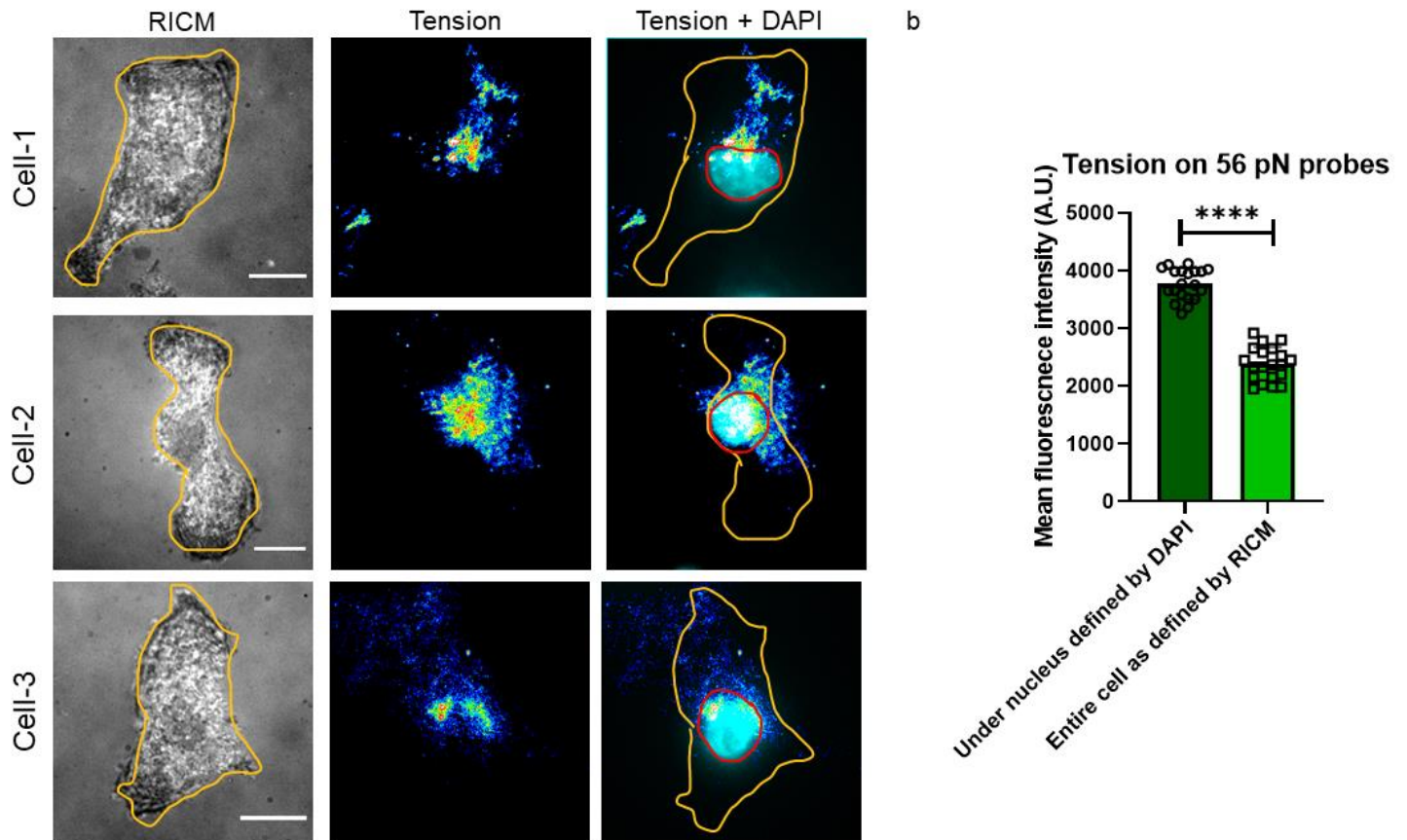
Supplementary Figure 8. Nuclear staining confirms tension puncta localization under nucleus on 56 pN probe. a) Three representative RICM, tension and tension + DAPI images of CMCs on 56 pN rupture probes. Nuclear ROI (red) was selected from DAPI channel and tension was measured by mean fluorescent intensity. For total tension cell outline was selected from RICM channel and mean fluorescent intensity was measured in the tension channel. b) Bar graph showing the comparison of nuclear tension vs peripheral tension, **** represents p<0.001, *n=3.* Scale bar= 10 μm.
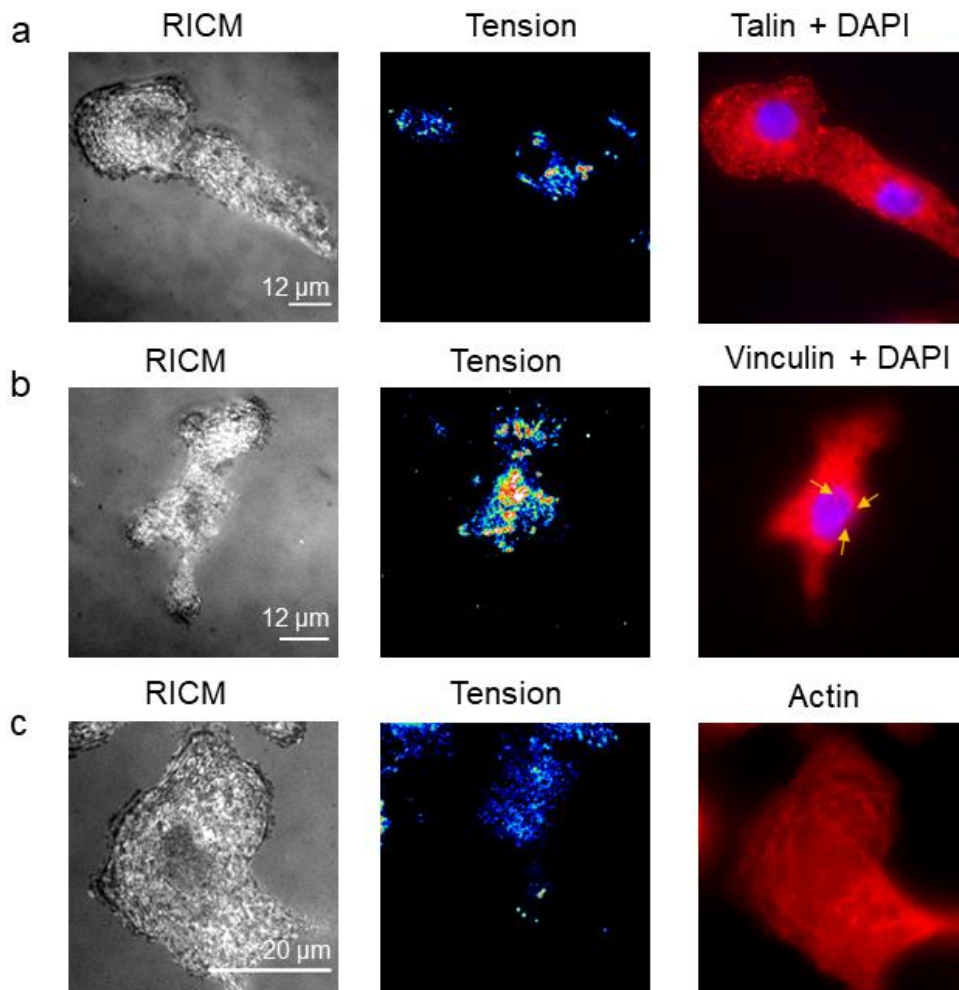
Supplementary Figure 9. Tension colocalization with Actin, talin and vinculin on 56 pN rupture probe. a-c. Representative RICM, tension and immunostaining for talin (a), vinculin (b) and actin (c).
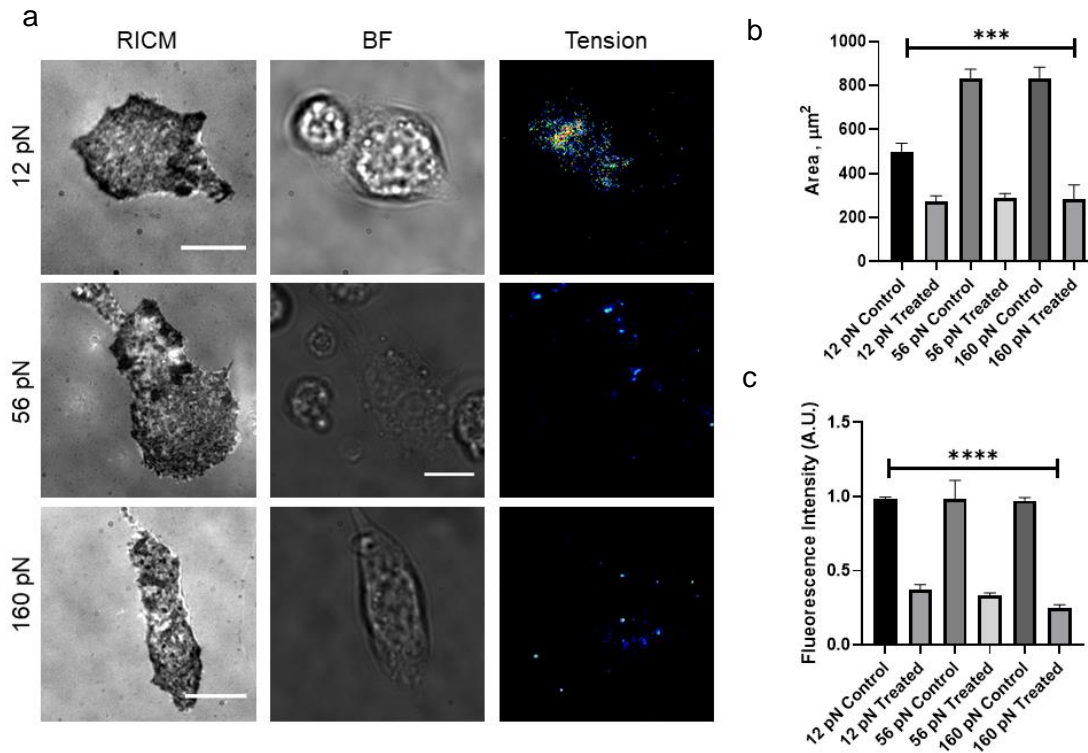
Supplementary Figure 10. Integrin inhibition (Eptifibatide) results in loss of force dependent functional maturation. a. Representative RICM, BF and Tension images of CMC on 12, 56, 160 pN probes treated with 10uM eptifibatide. b-c. Bar graphs showing the spread area and normalized tension (normalized to 12 pN control group) obtained from CMCs that were cultured on 12, 56 and 160 pN probes. Each data point represents a single cell while the bar shows the average. **** and *** indicate $p<0.0001$, $p<0.001$ respectively, as determined from one-way ANOVA. Error bars show standard deviation for *n*=3, where each experiment was averaged from three different cell isolations with three different sets of surface preparations. Scale bar=12 μm.
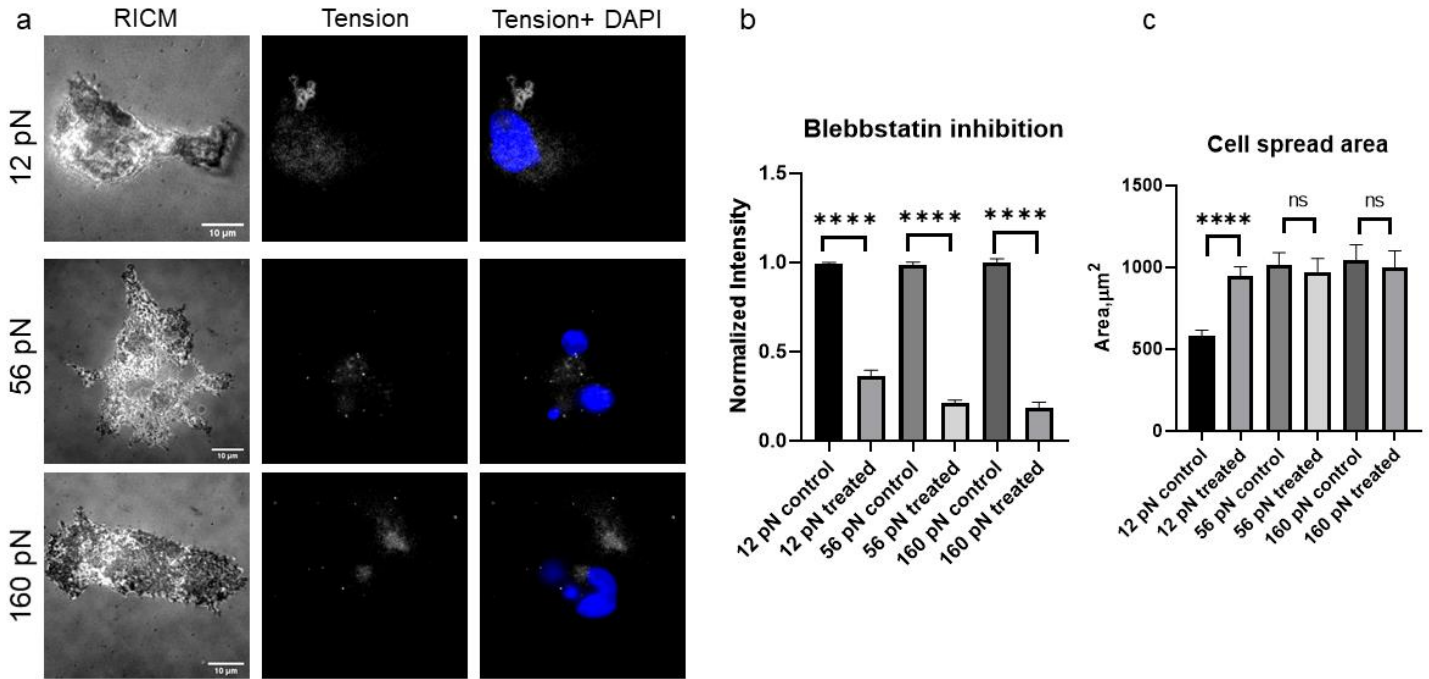
Supplementary Figure 11. Blebbstatin inhibition results in loss of force sensing driven functional maturation of CMCs. a. Representative RICM and Tension (TRITC) images of CMC on 12, 56, 160 pN probes treated with 25uM Y-27632. b-d. Bar graphs showing the spread area, aspect ratio, and the percentage of beating cells obtained from CMCs that were cultured on 12, 56 and 160 pN probes. Each data point represents a single cell while the bar shows the average. ****, ***, **, and * indicate $p<0.0001$, $p<0.001$, $p<0.01$ and $p<0.05$, respectively, as determined from one-way ANOVA. Error bars show standard deviation for $n=3$, where each experiment was averaged from three different cell isolations with three different sets of surface preparations. Scale bar=12 μm.
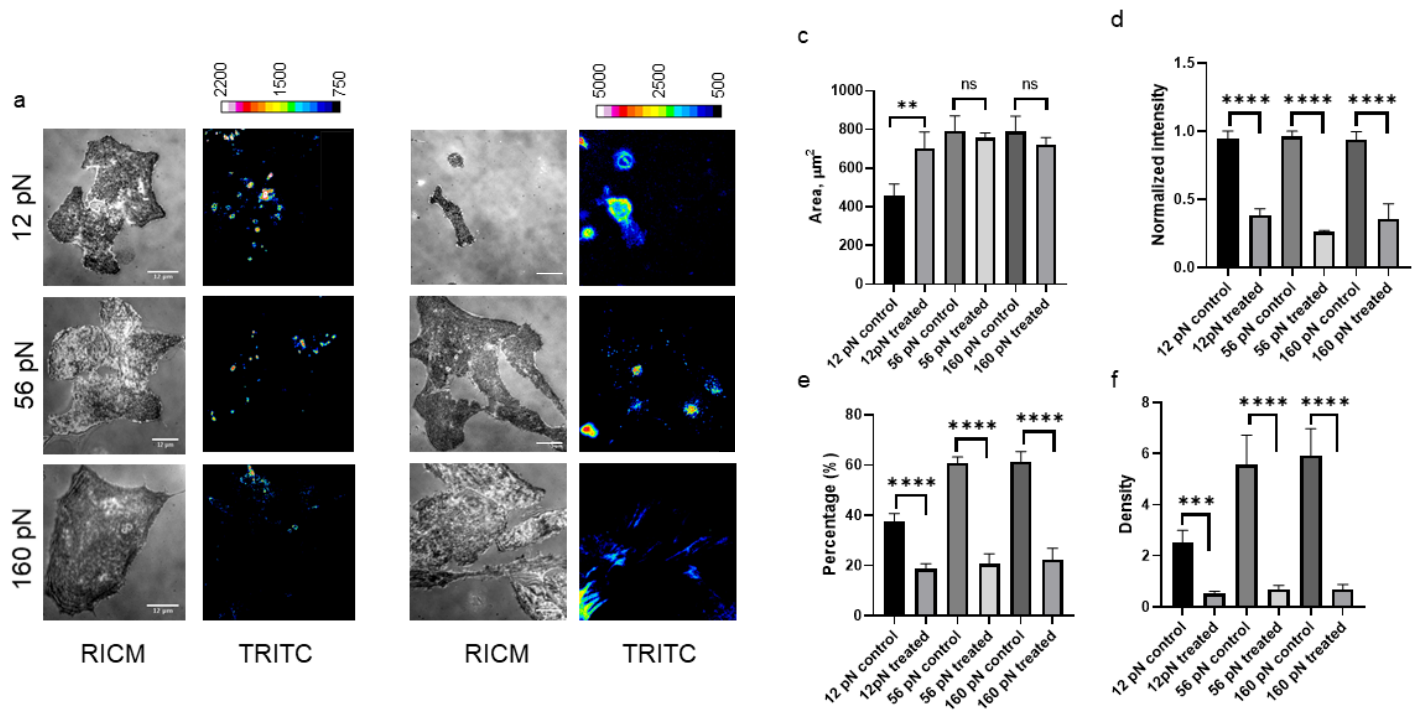
Supplementary Figure 12. ROCK inhibition results in loss of force sensing driven functional maturation of CMCs. a-b. Representative RICM and Tension (TRITC) images of CMC on 12, 56, 160 pN probes treated with and without(control) 25μM Y-27632. c-f. Bar graphs showing the spread area, normalized tension, the percentage of beating cells and density of attached cells obtained from CMCs that were cultured on 12, 56 and 160 pN probes. Each data point represents a single cell while the bar shows the average. ****, ***, **, and * indicate p<0.0001, p<0.001, p<0.01 and p<0.05, respectively, as determined from one-way ANOVA. Error bars show standard deviation for *n*=3, where each experiment was averaged from three different cell isolations with three different sets of surface preparations. Scale bar=12 *µ*m and 20 *µ*m .
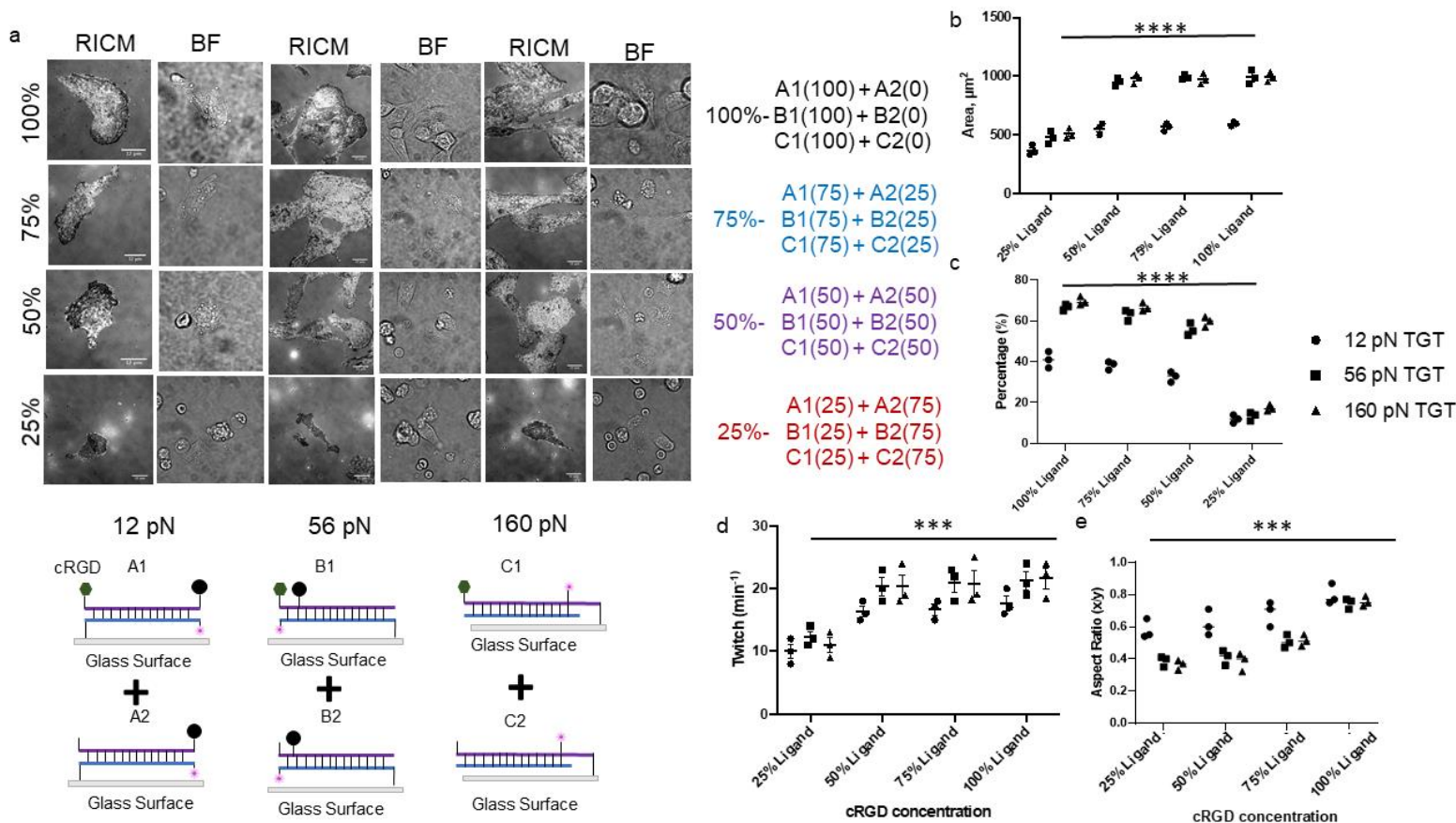
Supplementary Figure 13. Effect of ligand density on cell spreading area and beating frequency. a. Representative RICM and BF images of CMC on 12, 56 and 160 pN probes with four different ligand densities (100%, 75%, 50% and 25%). The different ligand densities were achieved by incubating the surface with a binary mixture of two probes: one lacking and the second displaying the RGD ligand. The total concentration of the probes was held at 150 nM to keep a constant DNA density on these surfaces. b. Scatter plot showing spread area of CMCs on 12, 56 and 160 pN probes having 100%, 75%, 50% and 25% ligand. The spread area was measured using RICM. **** indicates $p<0.0001$ from one-way ANOVA. Error bars show standard error of the mean for n=3, where each experiment was conducted from three different cell isolations with three different sets of surface preparations. Each experiment included over 20 cells that were analyzed. c-e. Scatter plot showing the percentage of beating CMCs, beating frequency and aspect ratio on surfaces of differing ligand density and rupture force (**** indicates $p<0.0001$ and *** indicates $p<0.01$, Error bars shows standard deviation for n=3, where each experiment was conducted from three different cell isolations with three different sets of surface preparations). Scale bar = 12 μm.

BF   Kymograph

4 s

10 µm

4 beats in 30s timelapse
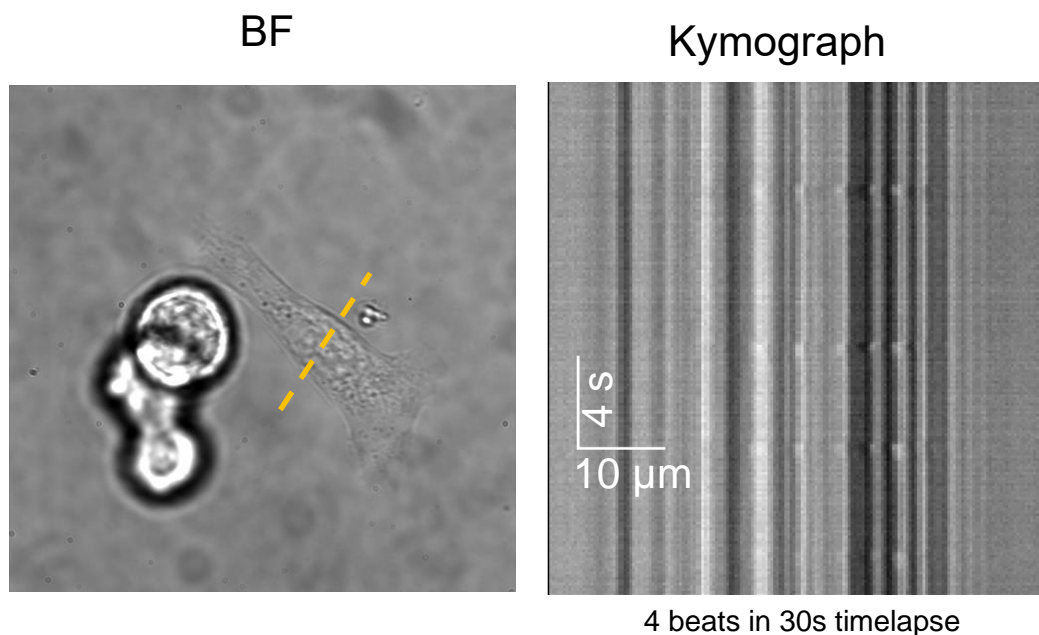
Supplementary Figure 14. Twitching frequency measurement. To measure the twitching frequency, we acquired a time-lapse video of CMC grown on the different DNA probe surfaces and determined the twitching frequency by using kymograph analysis. The data is reported in main **Figure 3b**. Here we show a snapshot from the time-lapse as well as a representative kymograph plot. The twitching frequency of the cells was measured by the "Multikymograph plot" plugin in ImageJ. To use the plugin, a line was drawn in the BF time-lapse image at the center of the twitching cells in the avi acquisition (towards the long axis). The horizontal line (indicated by the arrow) indicates the twitching of cell. the vertical distance is measured in unit of time(s) and the horizontal measurement shows displacement. Each horizontal line is counted as one beat and the time required was calculated by measuring the distance (vertical) from two neighboring lines. From each kymograph we measured three twitching frequencies (twitch/min) and averaged those values for each ROI.
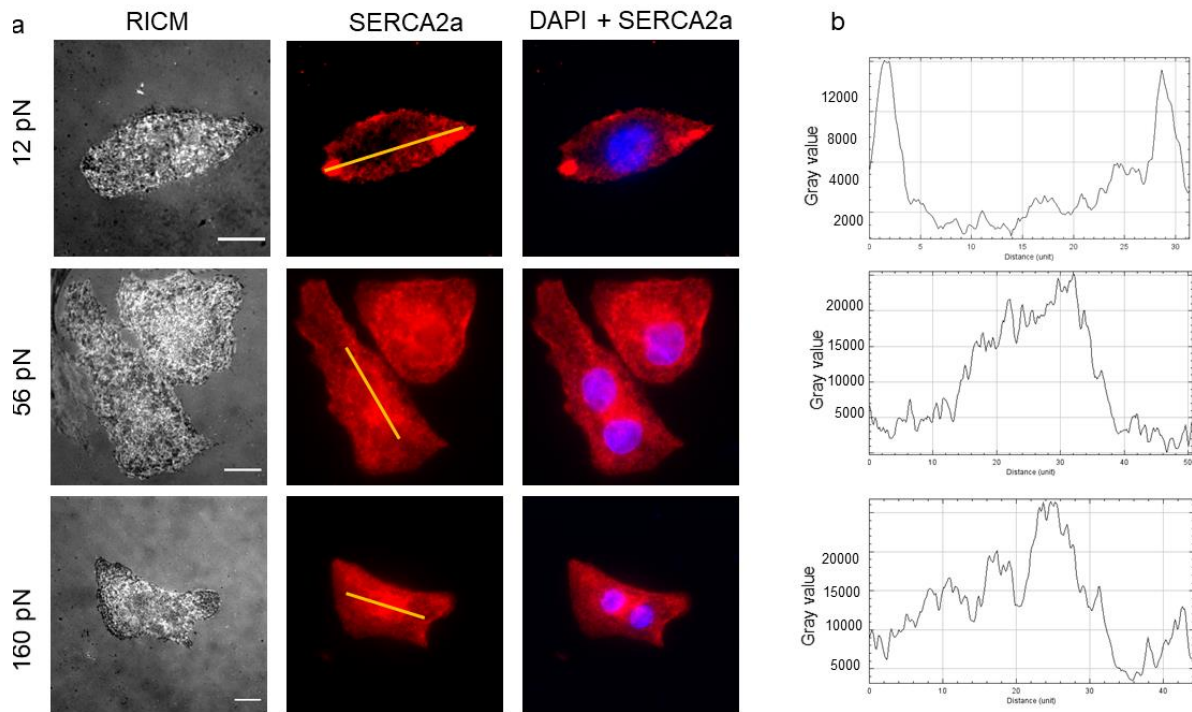
Supplementary Figure 15. Distribution of SERCA2a. a) Representative RICM, SERCA2a, SERCA2a+DAPI images of CMCs on 12 pN, 56 pN and 160 pN rupture probes. b) Line scan of the SERCA2a intensity (yellow line) shows SERCA is mostly localized in the center in CMCs on 56 and 160 pN rupture probes. Scale bar= 12 μm.
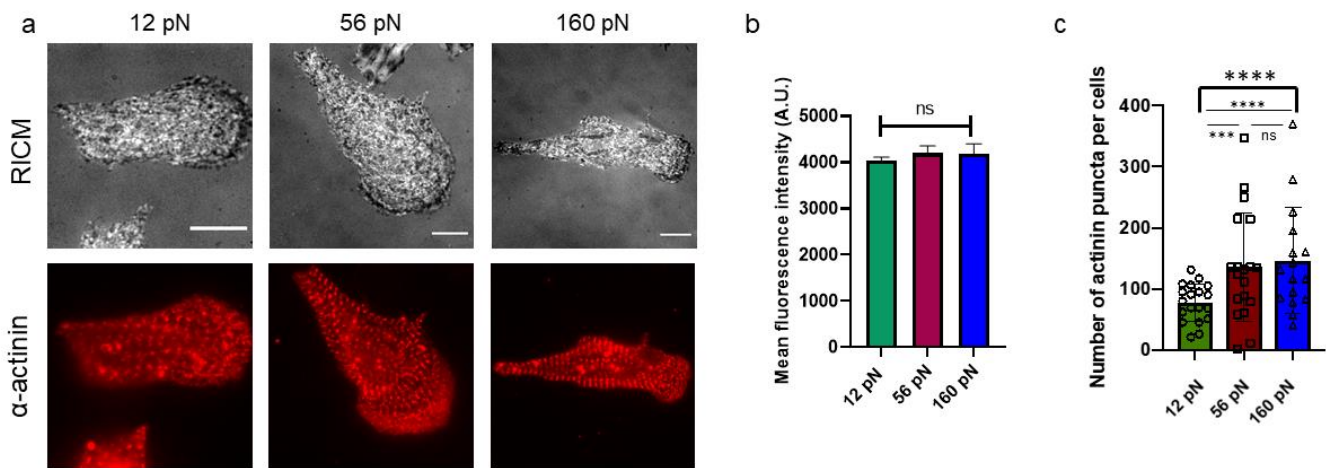
Supplementary Figure 16. α-actinin expression of CMCs on rupture probes a) Representative RICM and α-actinin images of CMCs on 12, 56 and 160 pN surfaces. Bar graph showing mean α-actinin expression. b) bar graph showing number of α-actinin puncta on 12, 56 and 160 pN rupture probes. *n=3*. Scale bar= 10 *μ*m. c) Number of actinin puncta per cell as measured by supplementary method 3.
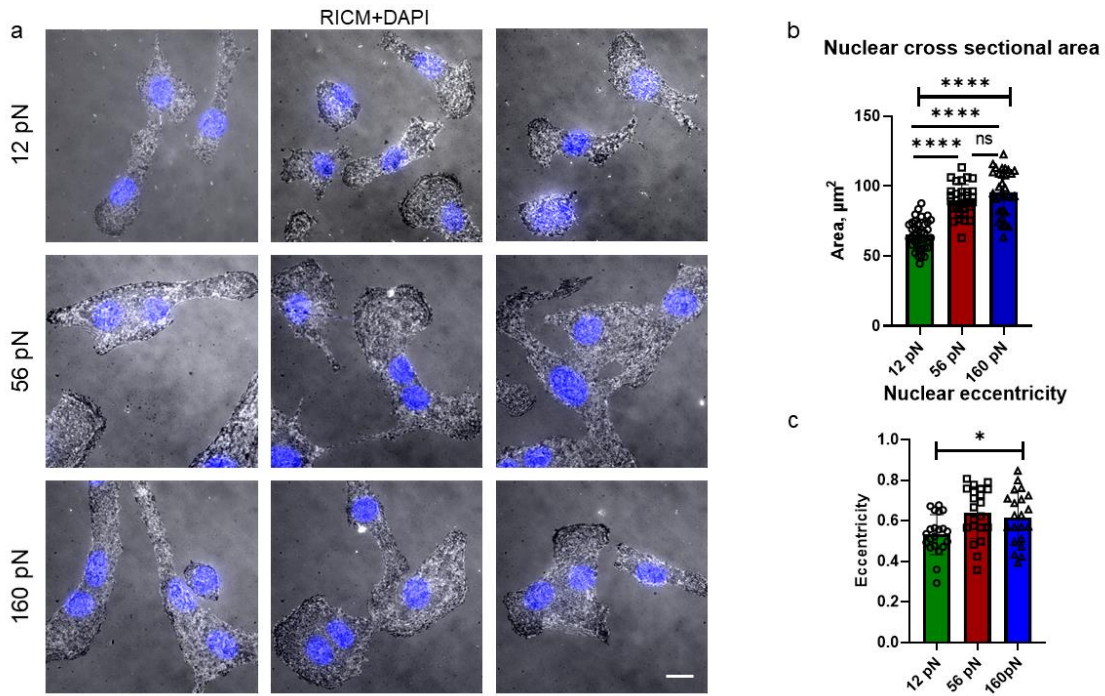
Supplementary Figure 17. Multinucleation on 56 and 160 pN probes. a. Representative RICM, BF and DAPI images of CMC on 12, 56, 160 pN probes stained with nucBlue for nucleus. CMCs on 56 and 160 pN surfaces had higher nuclear diameter and increased multinucleation. Scale bar=15 μm.
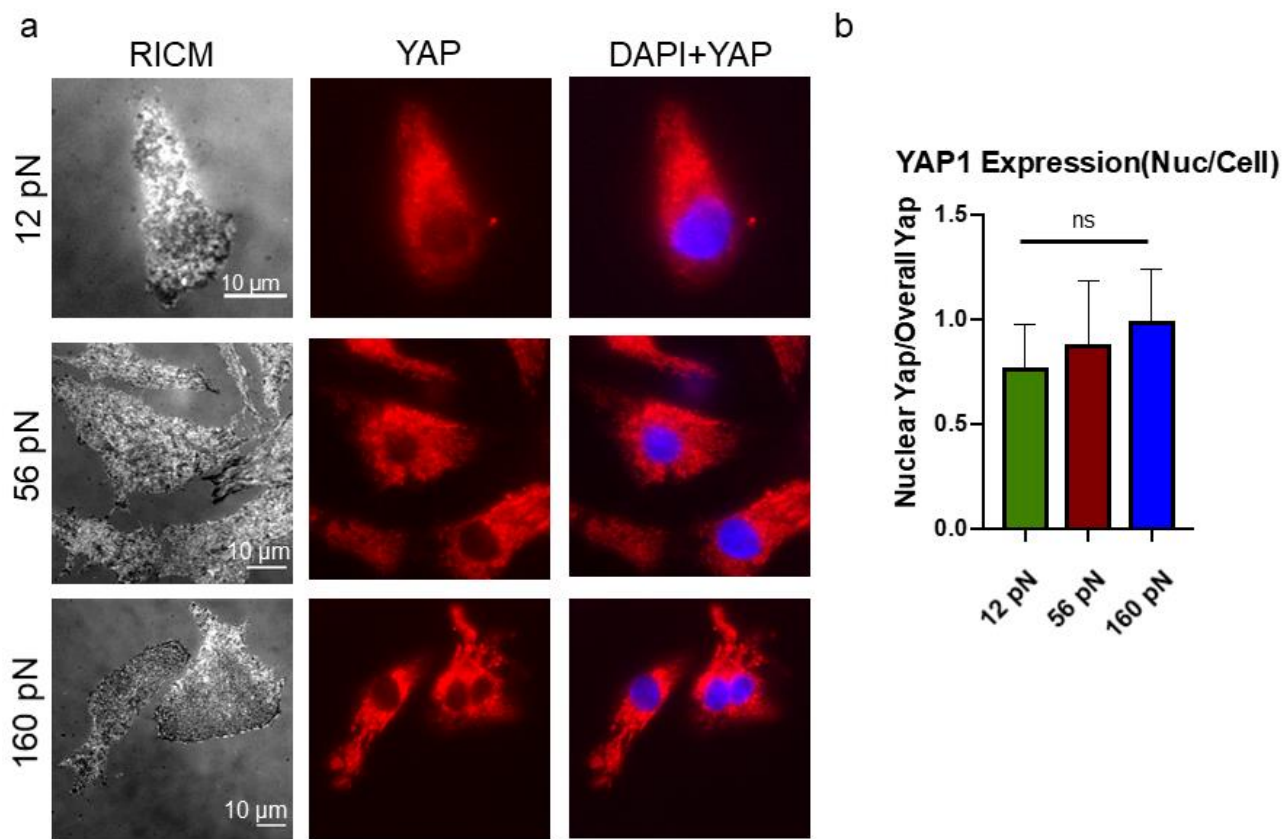
Supplementary Figure 18. YAP nuclear translocation is time dependent a. Representative RICM, YAP and YAP+DAPI images of CMCs grown on 12, 56, 160 pN probe surfaces(t=8-10 hrs). b. Bar graph plotting the Nuclear/ overall YAP (ns indicates statistically not significant from one-way ANOVA. Error bars show standard error of the mean for n=3, where each experiment was obtained from a unique cell isolation). Scale bar= 10 μm.
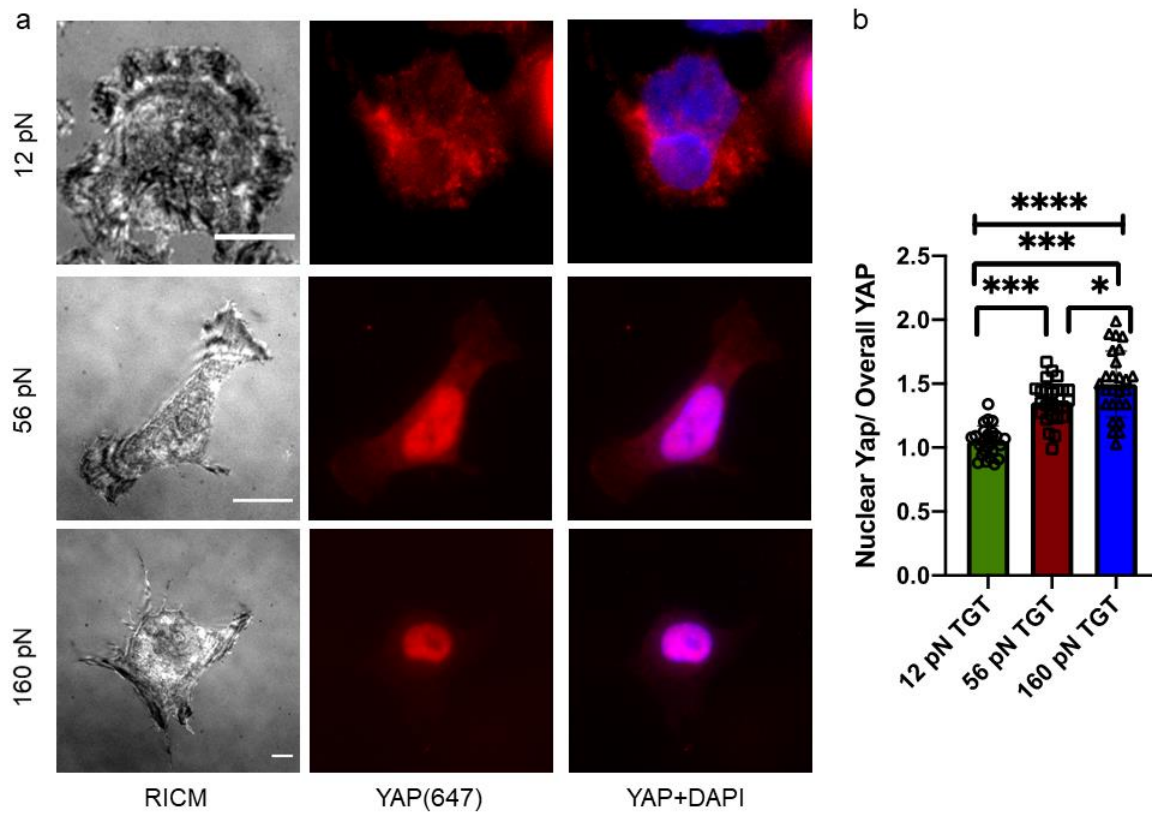
Supplementary Figure 19. CFs have an increased nuclear YAP on 160 and 56 pN probes with greater nuclear YAP signal on 160 pN probes compared to 12 pN probe. a. Representative RICM, YAP (647) and overlay of the DAPI (405) and YAP (647) images of CFs cultured on 12, 56, 160 pN probes. b. Bar graph plotting YAP nuclear translocation calculated by nuclear YAP/ overall YAP for CFs on 12, 56 and 160 pN probes. ****, *** and * indicates $p<0.0001$, $p<0.001$ and $p<0.05$ respectively, from one-way ANOVA. Error bars show the standard error of the mean for $n=3$, where each n experiment was obtained from unique cell isolations. Scale bar=5 μm.
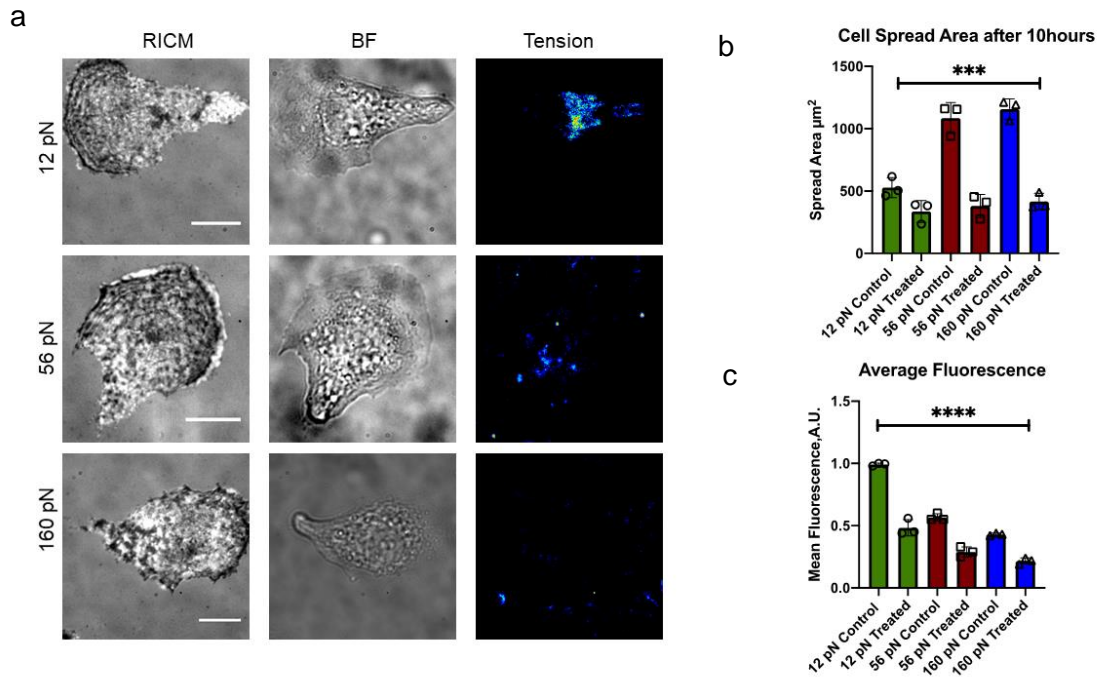
Supplementary Figure 20. MEK inhibition dampens integrin tension and force sensing of CMCs a. Representative RICM, BF and tension images of CMCs grown on 12, 56, 160 pN probe surfaces for cells pre-treated with 10 μM u1026. Cells were pretreated with drug for 30 min. b. Bar graph plotting the spread area of CMCs on three different probes. c. Bar graphs show the normalized tension (normalized with untreated CMCs tension on 12 pN probes). **** and *** indicates $p < 0.0001$ and $p < 0.001$ respectively, from one-way ANOVA. Error bars show standard error of the mean for n=3, where each experiment was obtained from a unique cell isolation. Scale bar= 10 μm.
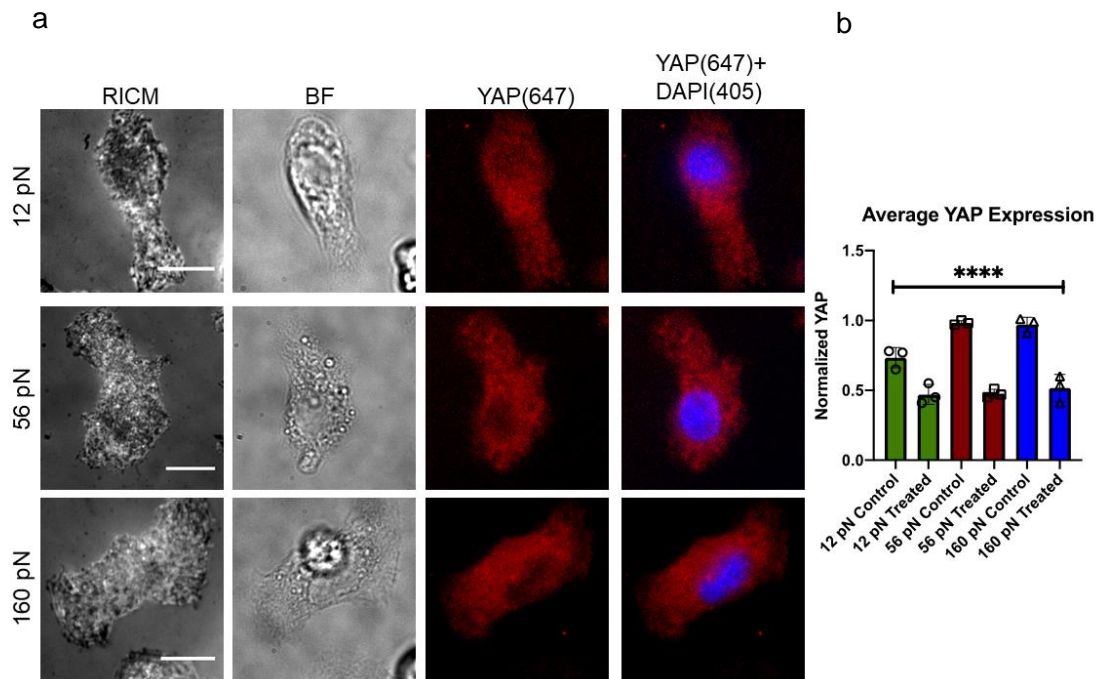
Supplementary Figure 21. MEK inhibition downregulates YAP expression of CMCs on all three different probes a. Representative RICM, BF, YAP (cy5) and overlay of DAPI and YAP images of CMCs on 12, 56, 160 pN probes. Cells were pre-treated with 10 μM u1026 for 30 min prior to plating. c. Bar graph shows the normalized YAP expression (normalized to untreated cells on the 160 pN probes). **** indicates $p<0.0001$ from one-way ANOVA. Error bars show standard error of the mean for n=3, where each experiment was obtained from a unique cell isolation. Scale bar=10 μm.
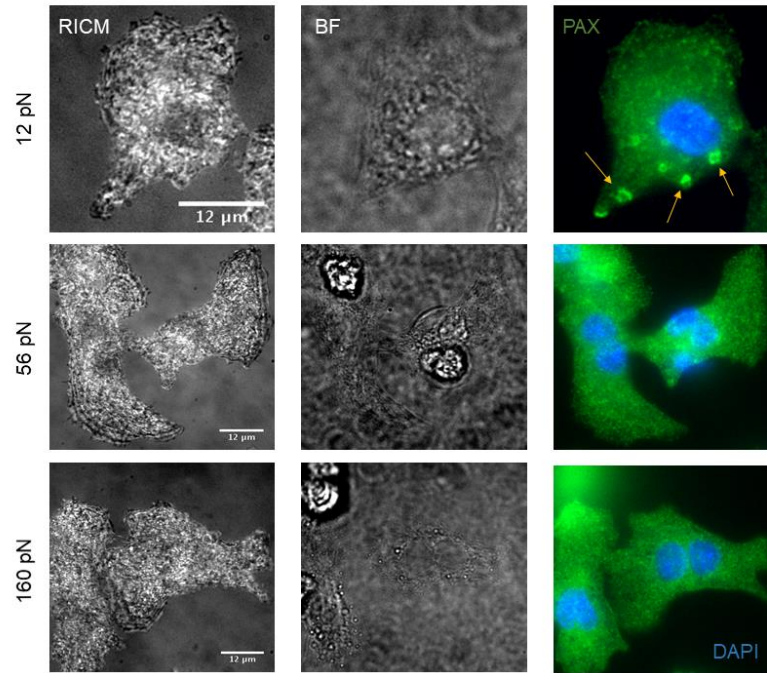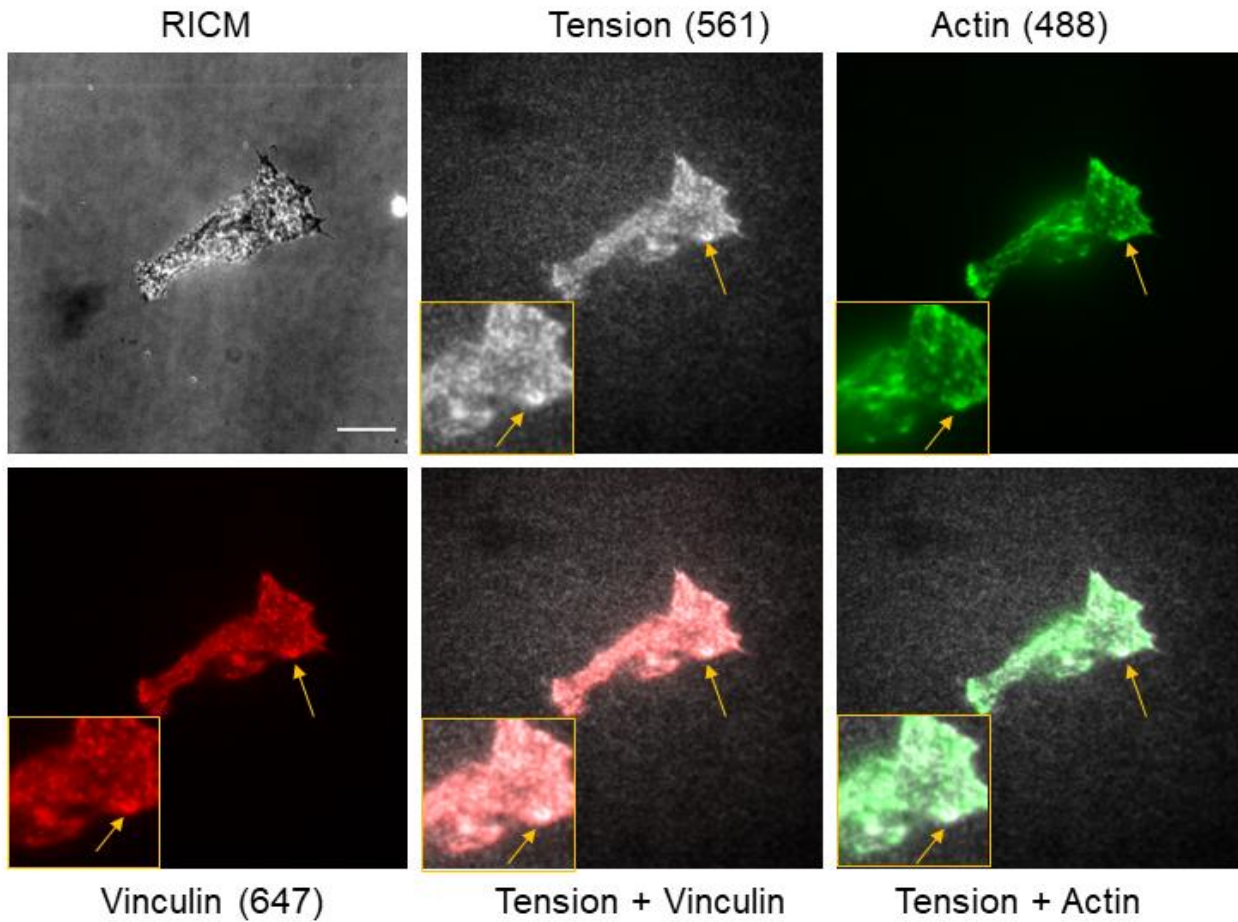
Supplementary Figure 22. **Paxillin staining confirms podosome like puncta on 12 pN probes**. Representative RICM, BF and DAPI+ FITC (paxillin) images of CMCs stained with phospho-paxillin antibody. CMCs on 12 pN had podosome like puncta on 12 pN probes compared to the 56 and 160 pN probes. Scale bar=12 μm.

Supplementary Figure 23. **Vinculin and Actin staining showing colocalized podosome like puncta on 12 pN probes.** Representative RICM, BF, tension, vinculin, actin, tension + vinculin and tension + actin respective images of CMC stained with phalloidin and vinculin antibody. Scale bar=20 μm.
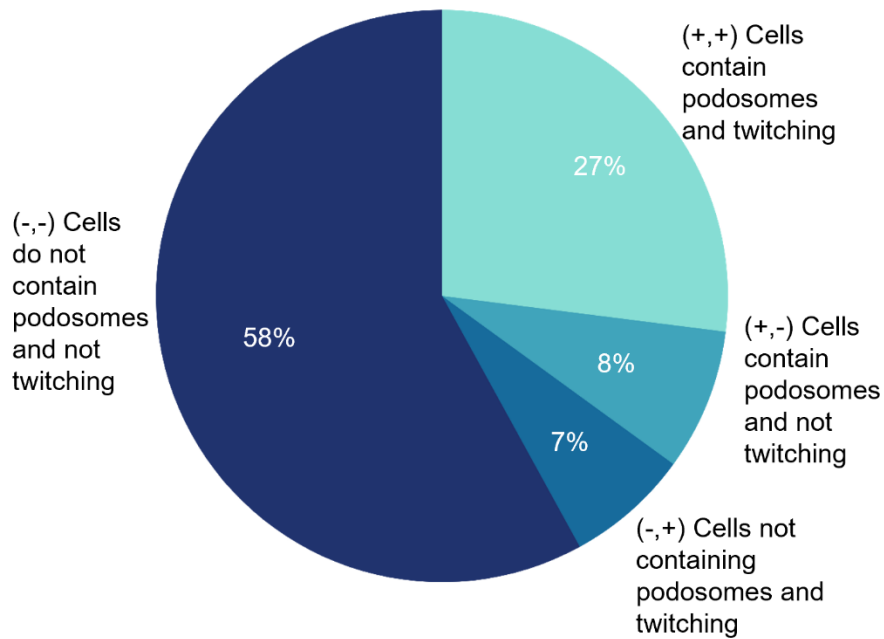
Supplementary Figure 24. Pie chart quantifying podosome formation and beating myocytes on 12 pN probes. The chart shows most of the CMCs that had contractility also had podosomes like organization. (From *n*>3, where cells were collected from three different isolation and three different sets of surface preparations).

Supplementary Figure 25. Podosome formation depends on the density of seeded cells. a. Representative RICM and tension images of podosome like structures that form under CMCs seeded on a 12 pN surface (2 hour after seeding). Scale bar= 5μm b. Representative RICM and tension images of densely seeded (~65,000) CMCs on 12 pN surface forming multiple podosomes near intercellular junctions. The red box indicates a region of interest with number of podosome like structures and the zoom-ins highlight this region. c-d. Bar graph plotting the number of podosomes and diameter of podosomes as a function of cell seeding density on 12 pN surfaces. (** indicates p<0.01 from one-way ANOVA. Error bars show standard error of the mean for *n*=3, where each experiment was obtained from unique cell isolations.
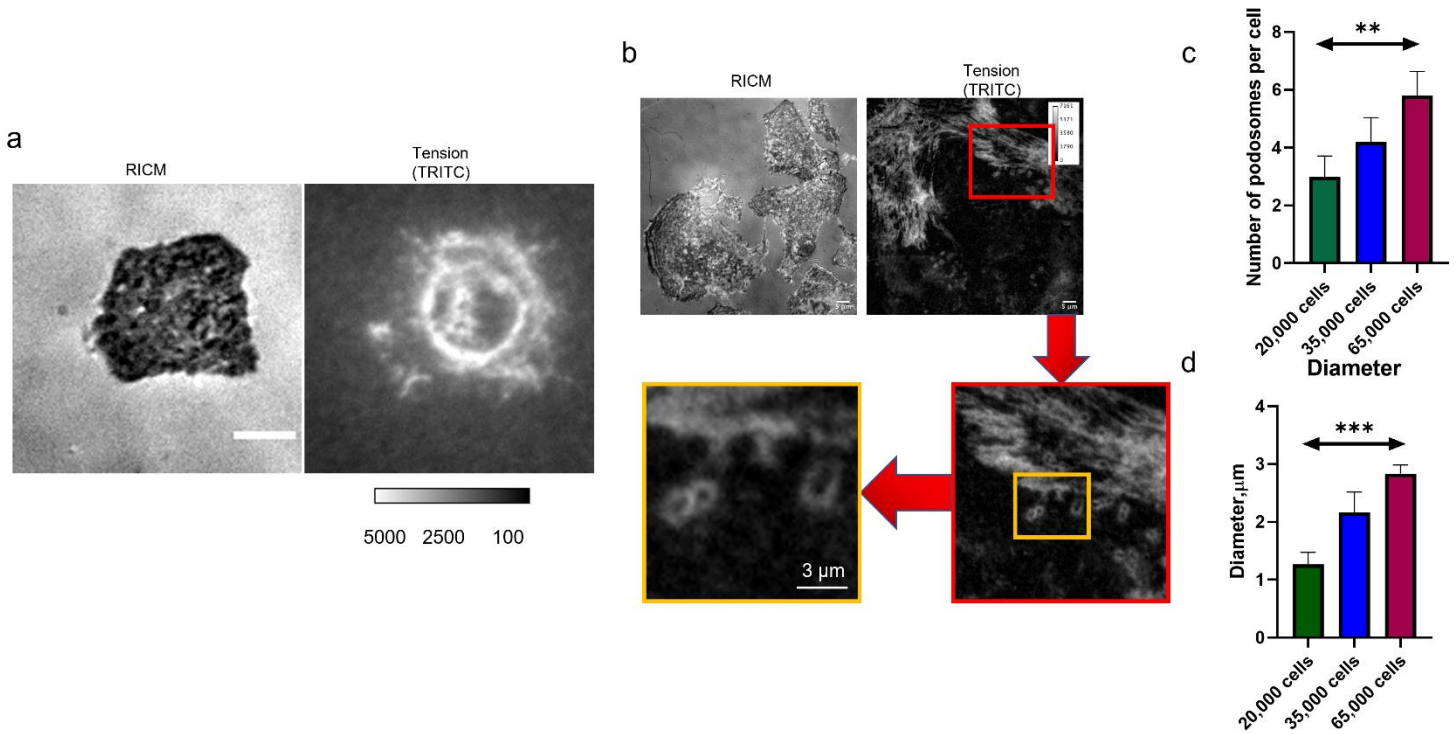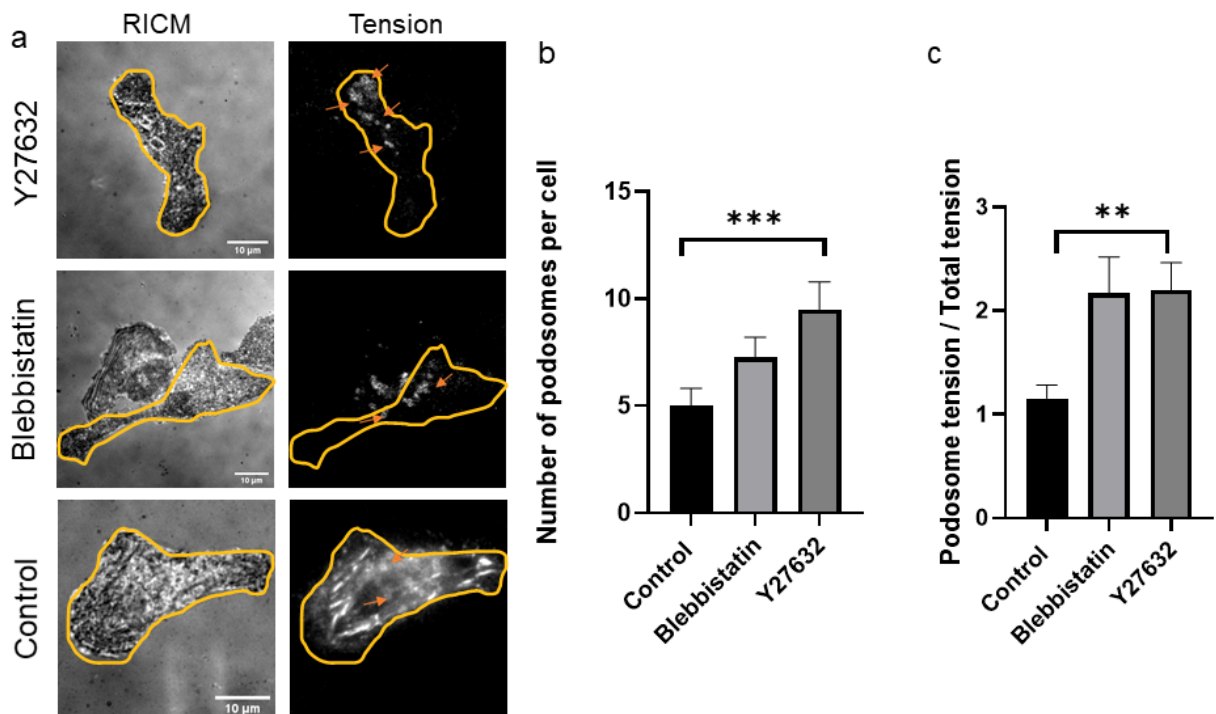
Supplementary Figure 26. Podosome formation is elevated on 12 pN surface when Tension is inhibited a. Representative RICM and tension images of podosome like structures that form under CMCs (either treated with Y27632, blebbistatin or just DMSO) seeded on a 12 pN surface. Scale bar= 10μm b. b-c. Bar graph plotting the number of podosomes and podosome tension/overall cell tension of CMCs on 12 pN surface (*** and ** indicates p<0.01 from one-way ANOVA. Error bars show standard error of the mean for *n*=3, where each experiment was obtained from unique cell isolations.
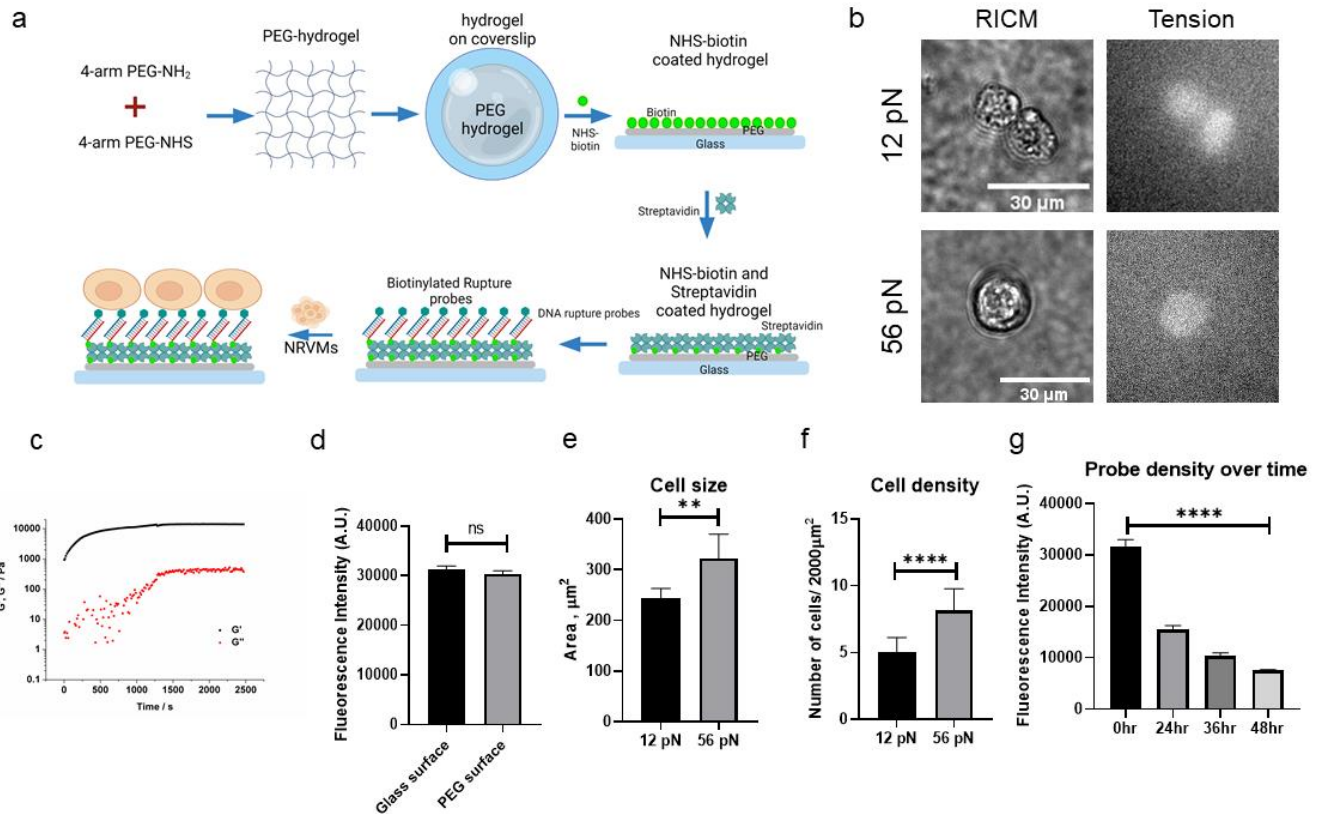
Supplementary Figure 27. CMCs did not elongate on TGT tethered PEG surface. a. Schematic representation of TGT coated PEG surface preparation. b. Representative BF and tension (Cy3B) images of CMCs on 12 and 56 pN TGT-PEG gels. c. Elastic modulus of 5 kDa- peg gel. d. Bar graph plotting the probe density (measure by surface fluorescence intensity) comparing conventional DNA probes linked to a glass slide and DNA-modified hydrogels. e and f. Plots showing cell size and cell density of CMCs on 12 and 56 pN TGT-PEG gel. The data was obtained from brightfield images. g. Bar graph plotting probe density as a function of time shows that DNA density decreases over 48hrs of CMCs incubation. **** and ** indicate $p<0.001$ and $p<0.01$ from one-way ANOVA. Error bars show standard error of the mean for n=3, where each experiment was obtained from unique cell isolations. Scale bar= 30 μm.

Supplementary Table-3: Representative list of past studies using hard substrates to study CMC biology.

1	Guo, Y.; Cao, Y.; Jardin, B. D.; Sethi, I.; Ma, Q.; Moghadaszadeh, B.; Troiano, E. C.; Mazumdar, N.; Trembley, M. A.; Small, E. M.; Yuan, G. C.; Beggs, A. H.; Pu, W. T., Sarcomeres regulate murine cardiomyocyte maturation through MRTF-SRF signaling. *Proc Natl Acad Sci U S A* **2021**, *118* (2).
2	Burbaum, L.; Schneider, J.; Scholze, S.; Bottcher, R. T.; Baumeister, W.; Schwille, P.; Plitzko, J. M.; Jasnin, M., Molecular-scale visualization of sarcomere contraction within native cardiomyocytes. *Nat Commun* **2021**, *12* (1), 4086.
3	Guo, Y.; Jardin, B. D.; Zhou, P.; Sethi, I.; Akerberg, B. N.; Toepfer, C. N.; Ai, Y.; Li, Y.; Ma, Q.; Guatimosim, S.; Hu, Y.; Varuzhanyan, G.; VanDusen, N. J.; Zhang, D.; Chan, D. C.; Yuan, G. C.; Seidman, C. E.; Seidman, J. G.; Pu, W. T., Hierarchical and stage-specific regulation of murine cardiomyocyte maturation by serum response factor. *Nat Commun* **2018,** *9* (1), 3837.
4	Kadota, S.; Minami, I.; Morone, N.; Heuser, J. E.; Agladze, K.; Nakatsuji, N., Development of a reentrant arrhythmia model in human pluripotent stem cell-derived cardiac cell sheets. *Eur Heart J* **2013,** *34* (15), 1147-56.
5	Wang, Z.; Cui, M.; Shah, A. M.; Ye, W.; Tan, W.; Min, Y. L.; Botten, G. A.; Shelton, J. M.; Liu, N.; Bassel-Duby, R.; Olson, E. N., Mechanistic basis of neonatal heart regeneration revealed by transcriptome and histone modification profiling. *Proc Natl Acad Sci U S A* **2019,** *116* (37), 18455-18465.
6	VanDusen, N. J.; Lee, J. Y.; Gu, W.; Butler, C. E.; Sethi, I.; Zheng, Y.; King, J. S.; Zhou, P.; Suo, S.; Guo, Y.; Ma, Q.; Yuan, G. C.; Pu, W. T., Massively parallel in vivo CRISPR screening identifies RNF20/40 as epigenetic regulators of cardiomyocyte maturation. *Nat Commun* **2021,** *12* (1), 4442.
7	Reid, B. G.; Stratton, M. S.; Bowers, S.; Cavasin, M. A.; Demos-Davies, K. M.; Susano, I.; McKinsey, T. A., Discovery of novel small molecule inhibitors of cardiac hypertrophy using high throughput, high content imaging. *J Mol Cell Cardiol* **2016,** *97*, 106-13.
8	O'Meara, C. C.; Wamstad, J. A.; Gladstone, R. A.; Fomovsky, G. M.; Butty, V. L.; Shrikumar, A.; Gannon, J. B.; Boyer, L. A.; Lee, R. T., Transcriptional reversion of cardiac myocyte fate during mammalian cardiac regeneration. *Circ Res* **2015,** *116* (5), 804-15.
9	Monroe, T. O.; Hill, M. C.; Morikawa, Y.; Leach, J. P.; Heallen, T.; Cao, S.; Krijger, P. H. L.; de Laat, W.; Wehrens, X. H. T.; Rodney, G. G.; Martin, J. F., YAP Partially Reprograms Chromatin Accessibility to Directly Induce Adult Cardiogenesis In Vivo. *Dev Cell* **2019,** *48* (6), 765-779 e7.
10	Huang, Q.; Huang, J.; Zeng, Z.; Luo, J.; Liu, P.; Chen, S.; Liu, B.; Pan, X.; Zang, L.; Zhou, S., Effects of ERK1/2/PPARalpha/SCAD signal pathways on cardiomyocyte hypertrophy induced by insulin-like growth factor 1 and phenylephrine. *Life Sci* **2015,** *124*, 41-9.
11	Li, J.; Gao, E.; Vite, A.; Yi, R.; Gomez, L.; Goossens, S.; van Roy, F.; Radice, G. L., Alpha-catenins control cardiomyocyte proliferation by regulating Yap activity. *Circ Res* **2015,** *116* (1), 70-9.
12	Feest, E. R.; Steven Korte, F.; Tu, A. Y.; Dai, J.; Razumova, M. V.; Murry, C. E.; Regnier, M., Thin filament incorporation of an engineered cardiac troponin C variant (L48Q) enhances contractility in intact cardiomyocytes from healthy and infarcted hearts. *J Mol Cell Cardiol* **2014,** *72*, 219-27.

Supplementary video 1. Representative time lapse showing bright field video of cardiomyocytes on 12 pN rupture probes after 6-8 hours of incubation. Videos were taken at 25fps for 1min. Scale bar = 10 μm

Supplementary video 2. Representative time lapse showing bright field video of cardiomyocytes on 56 pN rupture probes after 6-8 hours of incubation. Videos were taken at 25fps for 1min. Scale bar = 10 μm

Supplementary video 3. Representative time lapse showing bright field video of cardiomyocytes on 160 pN rupture probes after 6-8 hours of incubation. Videos were taken at 25fps for 1min. Scale bar = 10 μm

Supplementary video 4. Representative time lapse showing FITC video of cardiomyocytes stained with Fluo-4Am on 12 pN rupture probes. Cells were incubated for 6-8hours and stained for Ca^{2+} following aforementioned protocol. Videos were taken at 25fps for 1min. Scale bar = 50 μm

Supplementary video 5. Representative time lapse showing FITC video of cardiomyocytes stained with Fluo-4Am on 56 pN rupture probes. Cells were incubated for 6-8hours and stained for Ca^{2+} following aforementioned protocol. Videos were taken at 25fps for 1min. Scale bar = 50 μm

Supplementary video 6. Representative time lapse showing FITC video of cardiomyocytes stained with Fluo-4Am on 160 pN rupture probes. Cells were incubated for 6-8hours and stained for Ca^{2+} following aforementioned protocol. Videos were taken at 25fps for 1min. Scale bar = 50 μm

References

1. Bell, G. I., Models for the Specific Adhesion of Cells to Cells. *Science* **1978,** *200* (4342), 618-27.

2. Sedlak, S. M.; Bauer, M. S.; Kluger, C.; Schendel, L. C.; Milles, L. F.; Pippig, D. A.; Gaub, H. E., Monodisperse Measurement of the Biotin-Streptavidin Interaction Strength in a Well-Defined Pulling Geometry. *Plos One* **2017,** *12* (12), E0188722.

3. Mosayebi, M.; Louis, A. A.; Doye, J. P. K.; Ouldridge, T. E., Force-Induced Rupture of a DNA Duplex: From Fundamentals to Force Sensors. *ACS Nano* **2015,** *9* (12), 11993-12003.

4. Galush, W. J.; Nye, J. A.; Groves, J. T., Quantitative Fluorescence Microscopy Using Supported Lipid Bilayer Standards. *Biophys J* **2008,** *95* (5), 2512-9.

5. Pasqualin, C.; Gannier, F.; Yu, A.; Malecot, C. O.; Bredeloux, P.; Maupoil, V., Sarcoptim for Imagej: High-Frequency Online Sarcomere Length Computing on Stimulated Cardiomyocytes. *Am J Physiol Cell Physiol* **2016,** *311* (2), C277-83.